ARTICLE OPEN

Multifunctional-engineered NK cells overcome tumor immunosuppression by combining PD-L1 and HLA-E targeting and endogenous IL15 production

Piera Filomena Fiore[1], Sergio Forcelloni[1]✉, Lorenzo Moretta[2], Maria Rita Assenza[1], Paola Orecchia[3], Maria Teresa Bilotta[1], Markus Machwirth[4], Ted Shpati[4], Lokossou William Sanvi[4], Dorothee Haas[4], Simone Vitozzi[1], Manuela Giansanti[1], Francesca Nazio[5], Nicola Tumino[1]✉, Ignazio Caruana[4] and Paola Vacca[1]✉

The immunosuppressive tumor microenvironment (TME) poses a significant challenge to effective cancer immunotherapy, as it enables tumor escape through redundant checkpoint pathways, metabolic constraints, and direct inhibition of effector cells. To overcome these barriers, we developed a next-generation NK cell platform using a tri-cistronic retroviral vector that enhances NK cell activation, recruitment, survival, and metabolic fitness. Pan-cancer transcriptomic analyses reveal consistent co-expression of PD-L1 and HLA-E across tumors, which correlates with immune infiltration accompanied by strong immunosuppression, highlighting these molecules as key targets for immune evasion. To improve NK cell recruitment, activation, cytolytic function, survival, and metabolic fitness in the TME, we developed a next-generation NK cell platform using a tri-cistronic retroviral vector that encodes an extracellular PD-1 domain (^{ex}PD1) fused to the intracellular portion of NKG2D with the costimulatory molecule 4-1BB, and expressing soluble IL15 and NKG2A single-chain variable fragments (scFv). Thus, the ^{ex}PD1 allows the recognition of cells expressing PD-L1, while the intracellular costimulatory signaling transforms the inhibitory interaction PD-1/PD-L1 into an activating one. This strategy effectively targets PD-L1-positive tumor cells and induces de novo PD-L1 expression in otherwise negative tumors. To further enhance anti-tumor activity, we incorporated a module encoding soluble NKG2A-scFv to mask the NKG2A receptor on NK cells and hinder NKG2A/HLA-E inhibitory interaction. Additionally, we improved NK cell survival and expansion by delivering controlled low doses of IL15, which prevents NK cell exhaustion and extends their presence in vivo. This integrated strategy may provide a novel, ready-to-use allogenic mature NK cell therapy that could overcome checkpoint-mediated inhibition, metabolic suppression, and immune escape, offering a promising model for treating high-risk and treatment-resistant tumors.

Signal Transduction and Targeted Therapy (2026)11:269 ; https://doi.org/10.1038/s41392-026-02827-w

INTRODUCTION

Despite the significant and multifaceted progress achieved with multimodal cancer treatments, including surgery, radiotherapy, and targeted chemotherapy, and a much deeper understanding of the complex molecular underpinnings of tumor biology, the development of effective and durable therapies for patients suffering from advanced or metastatic tumors remains a major challenge.[1–6] In this context, the advent of immunotherapy has led to the clinical implementation of several diverse and transformative treatment strategies, including the systemic use of monoclonal antibodies (mAbs), therapeutic vaccines, and the adoptive transfer of engineered immune cells, which have collectively revolutionized modern medicine and significantly improved the five-year survival rates and overall patient outcomes.[5] However, clinical experience has shown that even the most advanced cellular approaches, such as chimeric antigen receptor (CAR) T cell therapies, often fail to achieve prolonged and sustained remission in patients with refractory (R/R) tumors. Thus, the development of new, more effective, and less toxic therapies is widely recognized by the scientific community as an urgent clinical need. This limited therapeutic efficacy primarily stems from the immunosuppressive nature of the tumor microenvironment (TME), the selective loss of target antigens, and the development of immune escape mechanisms orchestrated by the tumor.[7–9]

Key challenges in the clinical translation of CAR-T cell therapy include the limited number of functional autologous T cells obtained from pre-treated patients, the lengthy and labor-intensive time required for their production and expansion, high costs associated with individualized manufacturing, and the potential risk of severe toxicities.[1–3,10,11] Specifically, clinicians frequently encounter adverse events such as neurotoxicity and severe cytokine storms. In addition to these obstacles, the efficacy of tumor-specific mAbs and CAR-T cells is frequently further compromised by the tumor-driven loss of target antigens and the concomitant upregulation of immune checkpoint ligands, as well as the non-classical HLA-E molecule.[3,12–15] In particular, the overexpression of PD-L1 (CD274) on both tumor and stromal cells can inhibit effective immune responses through the target engagement of the PD-1 receptor, leading to

[1]Innate Lymphoid Cells Unit, Immunology Research Area, Bambino Gesù Children's Hospital IRCCS, Rome, Italy; [2]Tumor Immunology Unit, Bambino Gesù Children's Hospital IRCCS, Rome, Italy; [3]Ospedale Policlinico San Martino IRCCS, Azienda Ospedaliera Metropolitana (AOM), Genova, Italy; [4]Department of Paediatric Haematology, Oncology and Stem Cell Transplantation, University Hospital of Würzburg, Würzburg, Germany and [5]Department of Biology, University of Rome Tor Vergata, Rome, Italy
Correspondence: Sergio Forcelloni (sergio.forcelloni@opbg.net) or Nicola Tumino (nicola.tumino@opbg.net) or Paola Vacca (paola.vacca@opbg.net)

Received: 1 August 2025 Revised: 4 May 2026 Accepted: 18 May 2026
Published online: 10 July 2026

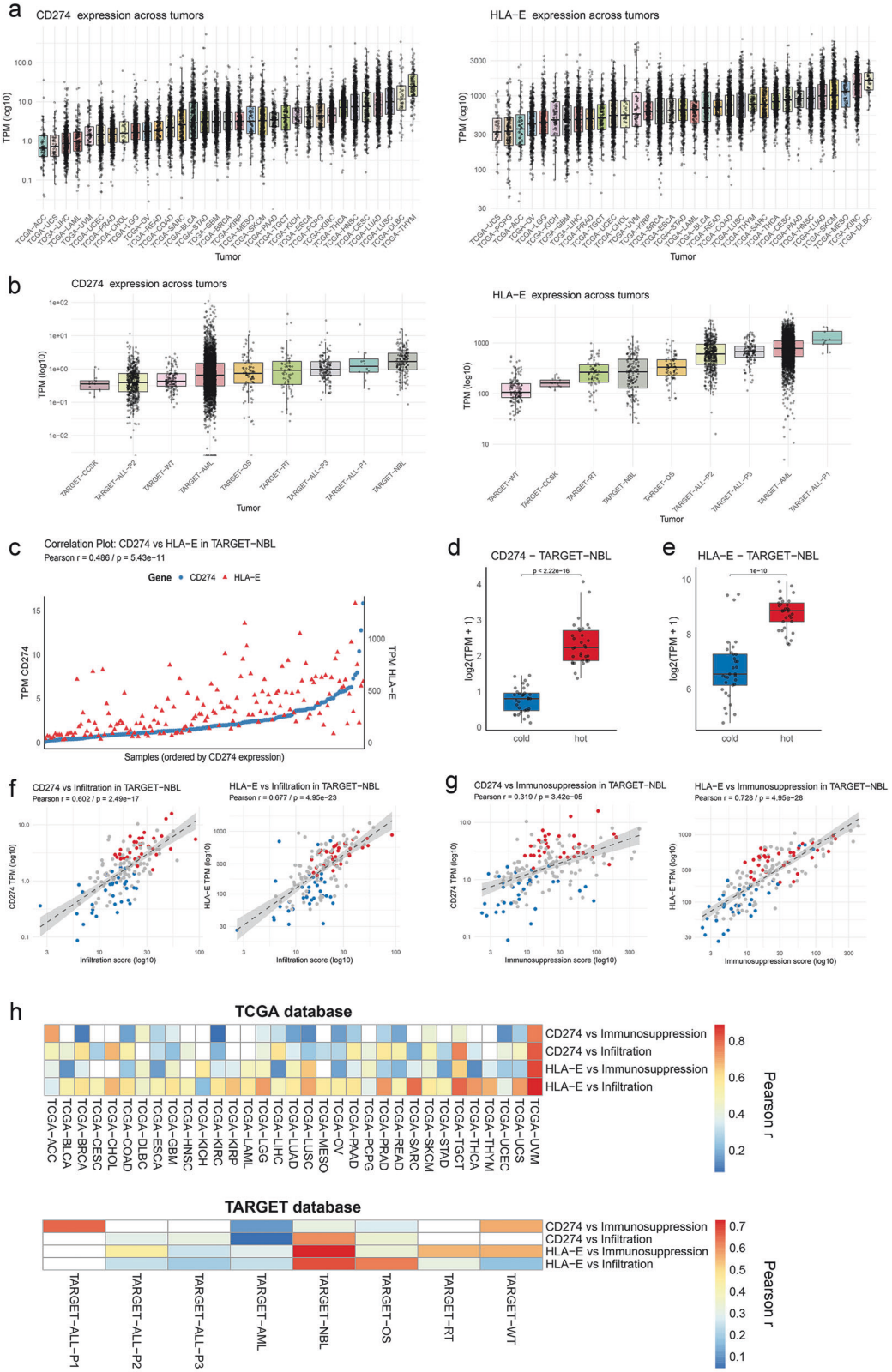

profound T cell dysfunction and irreversible exhaustion.[16] Conversely, it is important to note that while typically absent in healthy physiological states, only in pathological conditions characterized by chronic inflammation or malignancy, Natural Killer (NK) cells express PD-1 on their surface.[17,18] However, HLA-E expression on tumor cells may lead to suppression of NK cell activity upon interaction with the inhibitory heterodimer NKG2A/CD94 receptor complex.[15,19] Upon overcoming these regulatory and inhibitory limitations, NK cells appear as highly promising candidates for next-generation adoptive tumor immunotherapy.[7,20–24] Their innate and rapid cytotoxicity is strictly governed by a balance between activating and inhibitory receptors.[25]

Fig. 1 PD-L1 and HLA-E expression across tumor types and association with immune infiltration. **a**, **b** Expression of PD-L1 (CD274) and HLA-E in TCGA adult solid tumors and TARGET pediatric tumors (log_{10} TPM on the y-axis). **c** Correlation between PD-L1 and HLA-E expression in neuroblastoma (NBL); each dot represents one tumor sample, ranked by PD-L1 expression. P-value and Pearson correlation coefficient (r) are reported. Association of PD-L1 (**d**) and HLA-E (**e**) expression with immune infiltration score, defined by a cytotoxic lymphocyte gene signature. NBL tumors were stratified into "hot" and "cold" groups based on the upper and lower 20% of the immune infiltration score distribution. Both genes showed significantly higher expression in "hot" than in "cold" tumors (Wilcoxon rank-sum test). Correlation of PD-L1 and HLA-E expression with NK cell infiltration (**f**) and immunosuppressive gene signatures (**g**) in NBL. P-value and Pearson correlation coefficient (r) are reported. The dashed line represents the linear regression fit, with the shaded area indicating the 95% confidence interval. **h** Pan-cancer correlation analysis across TCGA adult tumors and TARGET pediatric tumors of PD-L1 and HLA-E expression with NK cell infiltration and immunosuppressive gene signatures. The heatmaps show Pearson correlation coefficients; colored squares indicate statistically significant positive correlations ($p \leq 0.05$), while white squares denote non-significant correlations ($p > 0.05$)

The biological advantages of NK cells over conventional T cells are substantial and offer new therapeutic avenues. Unlike T cells, NK cells recognize target cells in an antigen-independent manner. Importantly, allogeneic NK cells do not cause graft-versus-host disease (GvHD) or cytokine release syndrome (CRS), commonly associated with CAR-T treatments, thus offering a safer and more scalable "off-the-shelf" therapeutic alternative.[20] One of the main challenges in NK cell therapy is the achievement of an efficient and stable genetic modification and a robust clinical-grade expansion of NK cells to achieve therapeutic doses.[26,27] Indeed, current viral and non-viral transduction techniques remain suboptimal for primary NK cells, often resulting in low transgene expression levels.[28,29] To improve the overall therapeutic potential of NK cells, innovative protocols and optimized constructs are necessary to enhance cell proliferation, transduction rates, and scalability. To address these critical and outstanding challenges, we developed a new protocol to generate allogeneic, mature, and genetically modified ready-to-use NK cells.

Our next-generation NK cell engineering strategy aims to overcome the inhibitory signals of immune checkpoints within the hostile and nutrient-deprived tumor milieu. Specifically, our construct encodes an extracellular PD-1 ectodomain (^{ex}PD1) fused to stimulatory cytoplasmic domains, soluble NKG2A-specific single-chain variable fragment (scFv), and soluble IL15. Expression of ^{ex}PD1 on NK cells enables recognition of PD-L1 expressed by both tumor cells and tumor-associated (TA-) cells, effectively neutralizing the PD-1/PD-L1 axis. Meanwhile, secretion of NKG2A-scFv competitively blocks the NKG2A/HLA-E axis, alleviating TME-mediated suppression (which is known to express non-classical HLA-Class I molecules HLA-E) and preventing the mechanisms of tumor evasion. Then, the autocrine secretion of IL15 supports NK cell proliferation, survival, and sustained activity without the requirement for exogenous cytokine administration, which can often lead to systemic toxicity. This integrated molecular platform intrinsically enhances metabolic fitness, cellular survival, and tumor infiltration capacity, subverting the nutrient-deprived and immunosuppressive conditions typically found within the TME.[30] By optimizing the metabolic pathways, such as glycolysis and oxidative phosphorylation, these cells can persist longer in adverse conditions. Importantly, these engineered cells maintain cytotoxic function across diverse tumor types and exhibit potential to target both immune-infiltrated "hot" and non-infiltrated "cold" tumors.[31] This combined multitargeted approach may overcome the key barriers that limit current immunotherapies and further support the development of universal, off-the-shelf NK cell products with broad and potentially transformative clinical applicability across a wide spectrum of malignancies.

RESULTS

PD-L1 and HLA-E molecules are crucial for developing effective NK cell-based cancer treatments

To identify and develop a new and efficient strategy to improve NK cell-based immunotherapy, we focused on PD-L1 (CD274) and HLA-E, two key immunoregulatory ligands that are often upregulated by tumors to evade immune recognition.[32] We analyzed their expression across various adult and pediatric tumors using transcriptomic data from The Cancer Genome Atlas (TCGA) and Therapeutically Applicable Research to Generate Effective Treatments (TARGET) databases. Both PD-L1 and HLA-E genes were detected across different tumors (Fig. 1a, b). Moreover, their expression showed a significant positive correlation in neuroblastoma (NBL) (Fig. 1c), lung (LUAD), and pancreas (PAAD) tumors (Supplementary Fig. 1a).

Since these genes are induced by inflammatory cytokines and play a role in regulating immune escape, we hypothesized that their expression could correlate with immune cell infiltration and be associated with compromised functional activity. Thus, tumors were stratified into immune "hot" and "cold" groups using an immune score based on cytotoxic lymphocyte gene signature. Higher expression of PD-L1 and HLA-E was detected in "hot" tumors than in "cold" ones (Fig. 1d, e, and Supplementary Fig. 1b), confirming their association with tumor immune infiltration.

Next, we examined the relationship between PD-L1 and HLA-E expression and the NK cell-specific gene signatures associated with infiltration and immunosuppression. Both signatures showed a positive correlation with PD-L1 and HLA-E expression in all tumors analyzed (Fig. 1f–h and Supplementary Fig. 1c, d).

Overall, these results indicate that NK cells are present in hot tumors but may be functionally restrained by immunosuppressive mechanisms. Both PD-L1 and HLA-E appear to be frequently co-expressed in immune-infiltrated tumors and are likely to act in concert to suppress NK cell antitumor activity. These data highlight the therapeutic potential of simultaneously targeting the NKG2A-HLA-E axis and PD-L1 immune checkpoints to dampen NK cell inhibition, favoring anti-tumor responses.

Generation and characterization of ^{ex}PD1/NKG2A-scFv/IL15 vector

Based on the data above, to target the inhibitory interactions between tumor and effector cells, we designed a gamma (γ)-retroviral vector encoding a tri-cistronic construct that includes: *(i)* the extracellular domain of the PD-1 immune checkpoint (^{ex}PD1), *(ii)* a chimeric intracellular module combining NKG2D with the 4.1BB costimulatory domains, *(iii)* a soluble single-chain variable fragment (scFv) specific for NKG2A, and *(iv)* soluble IL15 (Fig. 2a). PD-1 expression allows the selective recognition of PD-L1-positive (PD-L1$^+$) cells, while the secretion of NKG2A-scFv offers an innovative and complementary strategy to disrupt the immunosuppressive NKG2A-HLA-E axis. Additionally, IL15 secretion supports and enhances NK cell metabolic fitness, survival, proliferation, and migration. Remarkably, the tri-cistronic γ-retrovirus is designed to co-express three distinct functional modules from a single transcript, utilizing self-cleaving 2 A peptide sequences to mediate equimolar but sequential protein expression. Importantly, the vector architecture imposes a hierarchical or positional effect on protein expression levels, often referred to as positional prioritization. In this system, the gene positioned first (^{ex}PD1) in the transcript exhibits the highest expression level, followed by the second (NKG2A-scFv) and third (IL15) genes,

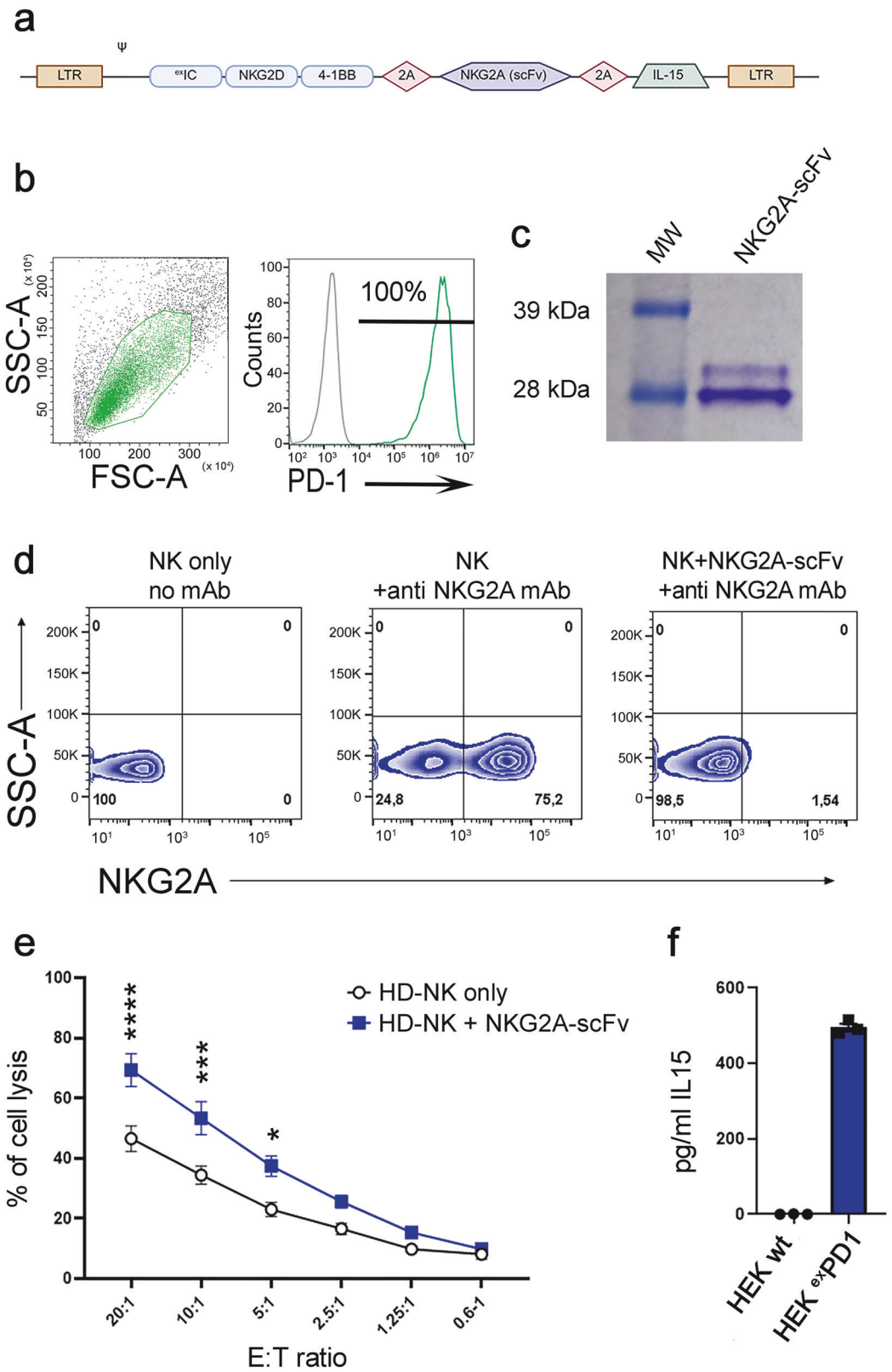

Fig. 2 Development of ^{ex}PD1/NKG2A-scFv/IL15 vector. **a** ^{ex}PD1/NKG2A-scFv/IL15 vector design scheme. **b** Representative flow cytometry analysis of PD-1 staining of transduced HEK-293T cells ($n = 5$). **c** SDS-PAGE showing NKG2A-scFv purified from supernatants of transfected HEK-293T cells. **d** Density plots indicating NKG2A expression on NK cells pre-incubated or not with purified NKG2A-scFv from the supernatant in transduced ^{ex}PD1-HEK-293T cells ($n = 5$). **e** Percentages of cell lysis (PI^+ cells) mediated by NK cells at different Effector:Target (E:T) ratios indicated, in the absence (white) or the presence (blue) of purified NKG2A-scFv. LCL 721.221.G cell line was used as the target cells. The results are expressed as means ± SEM of six different experiments using six different HD-NK cell donors. *p*-values were calculated using the 2-way ANOVA test for multiple comparison (*$p < 0.05$, ***$p < 0.001$, and ****$p < 0.0001$). **f** pg/ml of IL15 released by non-transduced HEK-293T cells (black bar) and ^{ex}PD1-HEK-293T cells (blue bar). The results are expressed as means ± SEM of 3 different experiments

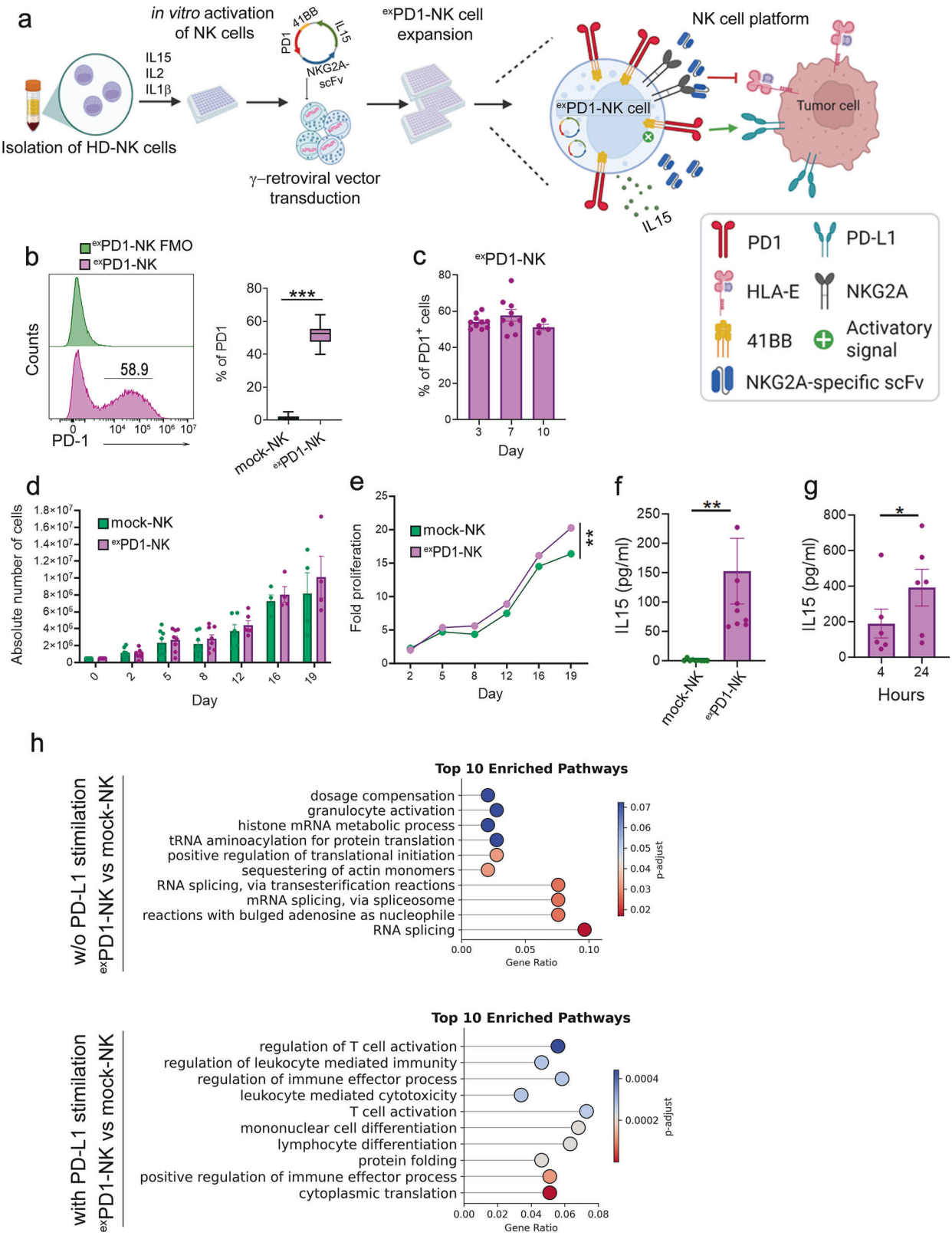

respectively. This specific arrangement of functional modules was chosen based on previous studies showing that a hierarchical structure ensures the production of each molecule at sufficient levels to improve therapeutic efficacy while preventing excessive expression that could result in toxicity.[28,33–37]

The functionality of the vector was initially assessed in HEK-293T cells. Upon transduction, these cells exhibited surface expression of exPD1, thus confirming the successful vector delivery and expression (Fig. 2b). To evaluate the production and secretion of NKG2A-scFv, culture supernatants from transduced HEK-293T cells

Fig. 3 Generation of ^{ex}PD1/NKG2A-scFv/IL15 NK cells. **a** NK cell expansion and transduction design experiment (generated by BioRender). **b** Representative histograms of PD-1 expression (left panel) in ^{ex}PD1-NK cells (pink line) and FMO as control (green line), and % of PD-1 expression obtained from 20 different experiments (right panel). *p*-value was calculated using the Wilcoxon t-test (***$p < 0.001$). **c** Percentages of PD-1^{+} cells at different time points (days) after transduction. The results are expressed as % of PD-1^{+} cells ± SEM of eight different NK cell donors. **d** Absolute numbers ± SEM of ^{ex}PD1- and mock-NK cells at different days of culture (starting from 5×10^5 at day 0 to day 19, $n = 4$–8). **e** Fold proliferation of ^{ex}PD1- and mock-NK cells ($n = 4$–8) from day 2 to day 19. 2-way ANOVA test for multiple comparison (**$p < 0.01$) was applied. **f** pg/ml ± SEM of IL15 released by mock- and ^{ex}PD1-NK cells (n = 8). *p*-value was calculated using the Wilcoxon t-test (**$p < 0.01$). **g** pg/ml ± SEM of IL15 released by ^{ex}PD1-NK cells at 4 and 24 hours ($n = 6$). *p*-value was calculated using the Wilcoxon t-test (*$p < 0.05$). **h** Top 10 significantly enriched GO biological processes based on proteins up-regulated in ^{ex}PD1- versus mock-NK cells before (upper panel) and after PD-L1 stimulation (lower panel). The lollipop plot shows the Gene Ratio on the x-axis, GO terms on the y-axis, and the adjusted *p*-value represented by the color scale

were collected and purified. Two protein fractions containing scFv were obtained. The second fraction, displaying a molecular weight of approximately 28 kDa, was consistent with the expected size of the NKG2A-scFv (Fig. 2c). Purified NKG2A-scFv was subsequently tested on NK cells from a healthy donor (HD) to evaluate its ability to compete for the binding of endogenous NKG2A with a fluorescently labeled anti-NKG2A mAb. HD-derived NK cells showed reduced or abrogated positivity for mAb binding after incubation with NKG2A-scFv, demonstrating its effective NKG2A receptor engagement (Fig. 2d). Next, to investigate the functional effect of NKG2A-scFv on the inhibitory effect of NKG2A-HLA-E interaction on tumor cells, HD-NK cells were pre-treated with purified NKG2A-scFv or untreated and tested for their ability to kill HLA-E^{+} LCL 721.221.G tumor cells. HD-NK cells incubated with NKG2A-scFv exhibited enhanced cytotoxicity in comparison to untreated NK cells (Fig. 2e), indicating that the released NKG2A-scFv effectively interfered with the NKG2A/HLA-E inhibitory interaction, restoring NK cell effector function. Finally, IL15 secretion was confirmed by analyzing supernatants from transduced HEK-293T cells. Unlike the wild-type (wt) cell line, only transduced cells released detectable levels of IL15, confirming the successful expression and secretion of all components of the tri-cistronic construct (Fig. 2f).

High-yield generation of functionally stable ^{ex}PD1-NK cells in vitro
A limitation in NK-based cellular therapy may be the difficulty in growing these cells in vitro. We established a protocol optimized for the rapid expansion and transduction of mature HD-NK cells from peripheral blood (PB). NK cells were isolated from the PB of HD and activated using IL1β, IL15, and IL2 cytokines. After three days of culture, NK cells were transduced with either the ^{ex}PD1 retroviral vector or an empty control vector (mock) (Fig. 3a). PD-1 expression was detected on NK cells at day 3 after the transduction (Fig. 3b) and remained stable over time (Fig. 3c). The ^{ex}PD1 expression was also preserved following cryopreservation and thawing (data not shown). Cell expansion was slightly higher in ^{ex}PD1-NK cells than in mock-NK cells, with a 20-fold increase versus 16-fold from the baseline (Fig. 3d, e). To evaluate the functionality of the PD1/4-1BB intracellular signaling domain, we stimulated ^{ex}PD1- and mock-NK cells with PD-L1 molecule and monitored the downstream signaling events. This analysis revealed phosphorylation of key signaling molecules (p-JNK, p-NFkB, and p-cJun) downstream of 4-1BB, indicating that engagement of the exogenous receptor leads to activation of this co-stimulatory pathway (Supplementary Fig. 2a). Additionally, the unique capability of ^{ex}PD1-NK cells to release the scFv specific for NKG2A was confirmed by observing its ability to mask NKG2A on ^{ex}PD1-NK cells, while NKG2A remained detectable on mock-NK cells (Supplementary Fig. 2b). Of note, when mock-NK cells were incubated with the ^{ex}PD1-NK cell-derived supernatant the expression of NKG2A was abrogated (Supplementary Fig. 2c) indicating that scFv could act both on ^{ex}PD1-NK cells and also on neighboring NK cells and other immune cells. Furthermore, the ^{ex}PD1-NK cells secreted IL15, different from mock-NK cells (Fig. 3f), the amount of IL15 increased over time in culture (Fig. 3g), and correlated to cultured cell concentration (Supplementary Fig. 2d). The amount of IL15 released by ^{ex}PD1-NK cells was relatively low, which reflects the positioning of the IL15 coding sequence in the third position (3rd) within the tri-cistronic vector. This hierarchical arrangement leads to lower IL15 expression compared to constructs with IL15 located in second (2nd), position (Supplementary Fig. 2e). The positioning of IL15 in the third position was designed to allow ^{ex}PD1-NK cells to produce IL15 in concentrations sufficient to support both their and allogenic HD-NK cell proliferation and survival (Supplementary Fig. 2f, g), minimizing the risk of potential adverse effects associated with excessive cytokine production.

To dissect the contribution of each component within the tri-cistronic construct, we generated modified vectors in which the NKG2A-specific scFv and/or IL15 were replaced with irrelevant proteins, while preserving the original gene order and expression hierarchy (Supplementary Fig. 2h). Proliferation assays were performed using vectors lacking IL15 alone (^{ex}PD1-NK $^{w/o\ IL15}$) or both IL15 and the NKG2A-specific scFv (^{ex}PD1-NK $^{w/o\ NKG2A/IL15}$). As an additional control, the ^{ex}PD1 vector (containing IL15) was evaluated in the presence or absence of a neutralizing anti (α)-IL15 monoclonal antibody (mAb). Under transwell conditions (Tw), ^{ex}PD1-NK cells promoted the proliferation of allogeneic HD-NK cells, supporting their survival. This effect was significantly reduced in the presence of αIL15 mAb. In contrast, NK cells transduced with the IL15-deficient vector (^{ex}PD1-NK$^{w/o\ IL15}$) failed to sustain the proliferation of allogeneic HD-NK cells. Similarly, the tri-cistronic vector lacking both IL15 and the NKG2A-scFv (^{ex}PD1-NK$^{w/o\ NKG2A/IL15)}$ did not induce HD-NK proliferation (Supplementary Fig. 2i, j). Collectively, these findings indicated that IL15 production by ^{ex}PD1-NK cells is important for both autocrine and paracrine support of NK cell survival, underscoring its functional relevance even at relatively low expression levels within the tri-cistronic configuration.

To evaluate the contribution of the NKG2A-specific scFv, we generated vectors in which this component was replaced with an irrelevant protein (Supplementary Fig. 2h). As shown in Supplementary Fig. 2k, the tri-cistronic vector lacking the NKG2A-specific scFv (indicated as ^{ex}PD1-NK$^{w/o\ NKG2A}$) exhibited reduced cytotoxicity against neuroblastoma target cells in a 4 hour cytotoxicity assay. This is likely due to the lack of blockade of the inhibitory NKG2A/HLA-E interaction, which allows inhibitory signaling to persist and limits NK cell-mediated tumor lysis. Notably, the vector lacking both IL15 and the NKG2A-specific scFv showed a further decrease in cytotoxicity, consistent with the proliferation data (Supplementary Fig. 2i–k). These results highlight the cooperative contribution of all components within the tri-cistronic construct in enhancing both the survival capacity and antitumor function of genetically modified ^{ex}PD1-NK cells.

To assess the functional and molecular adaptations driven by the engineered receptor engagement under relevant conditions, we stimulated ^{ex}PD1- and mock-NK cells with the PD-L1 ligand. Proteomic analysis showed a broad upregulation of multiple functional pathways related to cell activation, cytotoxicity, and protein translation/folding in PD-L1-stimulated ^{ex}PD1-NK cells as

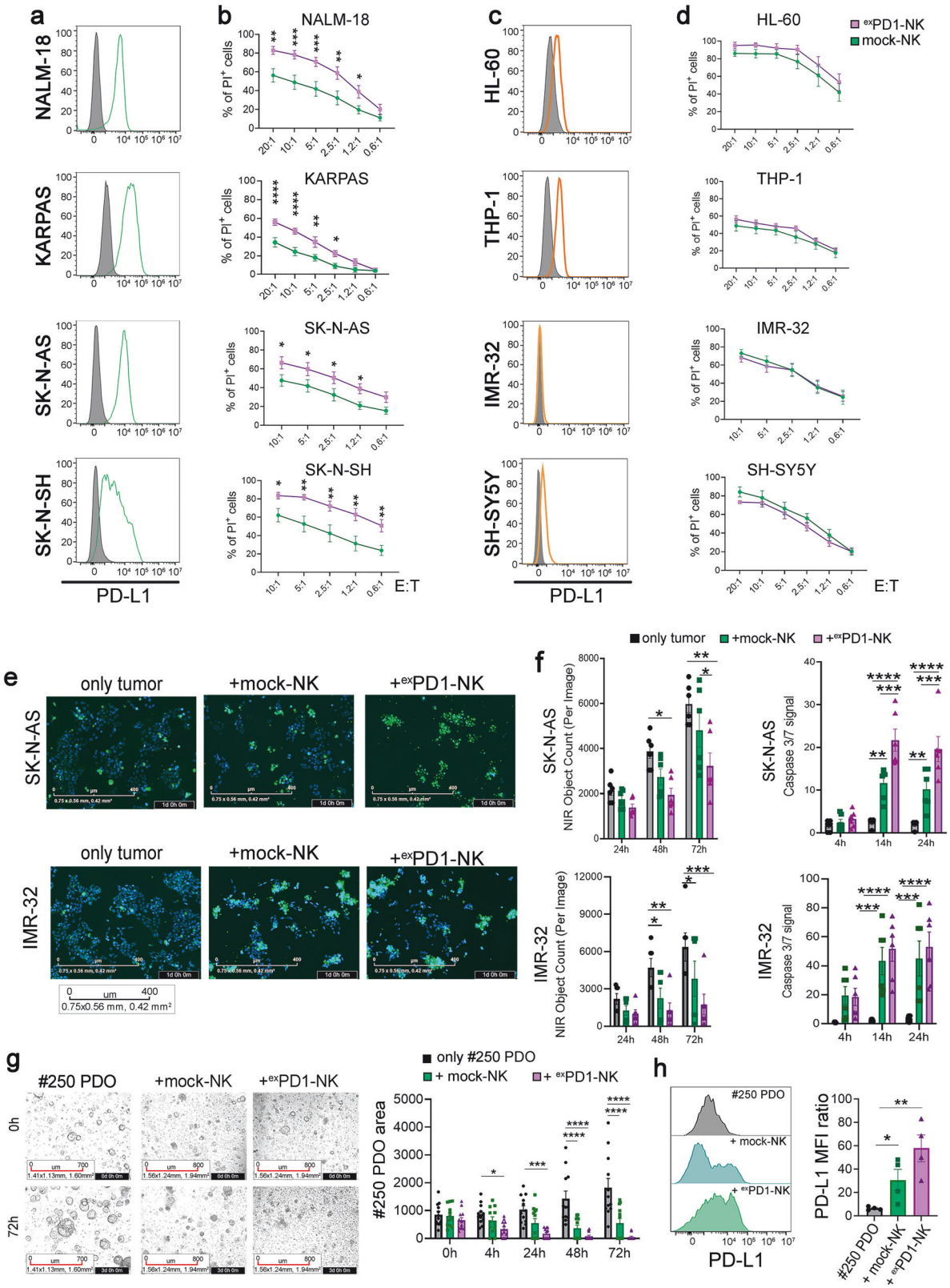

compared to mock-NK cells (Fig. 3h). In contrast, when PD-L1 stimulation was absent, the typical activation programs were not triggered. However, some molecular changes related to cell activation biology were observed in ^{ex}PD1-NK cells compared to mock-NK cells, despite the absence of PD-L1 stimulation (Fig. 3h). Moreover, Gene Set Enrichment Analysis (GSEA) revealed that the leading genes within several significantly enriched gene sets were related to effector functions, migration, adhesion, intracellular trafficking, and proliferation. This increase suggests that ^{ex}PD1-NK cells are more prone to infiltrate and kill solid tumor tissues as well as to establish effective immunological synapses (Supplementary Fig. 3a).

Fig. 4 Cytotoxic activity of ^{ex}PD1-NK cells. **a**, **c** PD-L1 expression (green and orange lines) on hematological and solid tumor cell lines. **b**, **d** Percentages ± SEM of cell lysis (PI^+ cells) mediated by ^{ex}PD1- (pink lines) and mock-NK (green lines) cells at different E:T ratios using the indicated target tumor cells ($n = 7$). *p*-values were calculated using the 2-way ANOVA test for multiple comparison (*$p < 0.05$, **$p < 0.01$, ***$p < 0.001$, and ****$p < 0.0001$). **e** Incucyte live imaging using NIR-nuclei (blue) to indicate tumor cells and caspase-3/7 dye (green) to indicate early apoptosis. SK-N-AS and IMR-32 cell lines were cultured alone, in the presence of mock- or ^{ex}PD1-NK cells. **f** Count of tumor cells and percentages of Caspase 3/7 of tumor cells cultured alone (black bars), in the presence of mock- (green bars) or ^{ex}PD1- (pink bars) NK cells at the indicated time points (means ± SEM of six independent experiments). *p*-values were calculated using the 2-way ANOVA test for multiple comparison (*$p < 0.05$, **$p < 0.01$, ***$p < 0.001$, and ****$p < 0.0001$). **g** Representative bright-field images and quantification area of PDOs (#250 patient) cultured alone or with mock- or ^{ex}PD1-NK cells at the indicated time-points. Mean ± SEM of 3 experiments using 4 different NK cell donors. *p*-values were calculated using a 2-way ANOVA test for multiple comparison (*$p < 0.05$, ***$p < 0.001$, and ****$p < 0.0001$). **h** Flow cytometry analysis of PD-L1 expression on #250 PDO, one representative histogram, and bar graphs showing the mean fluorescence intensity (MFI) ± SEM of 4 experiments using 4 different NK cell donors. *p*-values were calculated using the Mann-Whitney t-test (*$p < 0.05$ and **$p < 0.01$)

Finally, to evaluate the safety of viral gene transfer on NK cell phenotype and function, we assessed the expression of key activating NK cell receptors involved in tumor cell-recognition and lysis. The gene transfer did not affect the surface expression of NKp46, NKp44, NKp30, NKG2D, and DNAM-1 activating receptors (Supplementary Fig. 3b). Additionally, the gene expression profile revealed no significant changes in transcripts associated with NK cell-mediated anti-tumor activity (Supplementary Fig. 3c).

These results provide evidence of the efficient generation and transduction of large numbers of HD-derived mature ^{ex}PD1-NK cells within a short culture period, supporting the potential clinical applicability and scalability of this approach.

^{ex}PD1-NK cells exhibit strong antitumor activity against different hematological and solid tumors

To evaluate the effect of ^{ex}PD1 transduction on NK cell-mediated anti-tumor activity, we tested their cytotoxic activity against a panel of pediatric and adult tumor cell lines with different PD-L1 expression levels. The hematological NALM-18 and KARPAS cell lines, the neuroblastoma SK-N-AS and SK-N-SH cell lines, showed high PD-L1 expression (Fig. 4a). In contrast, the hematological cells HL-60 and THP-1, as well as the neuroblastoma IMR-32 and SH-SY5Y cell lines, displayed low or undetectable PD-L1 expression (Fig. 4c). Notably, all tested tumor cell lines expressed high levels of HLA-E on their surface (Supplementary Fig. 4).

After 4 hours of co-culture, ^{ex}PD1-NK cells displayed a significantly higher cytotoxicity against PD-$L1^+$ tumor cells than mock-NK cells (Fig. 4b). In contrast, both ^{ex}PD1- and mock-NK cells showed similar killing efficiency against PD-$L1^-$ tumor cells (Fig. 4d). These results suggest that ^{ex}PD1-NK cells have a rapid and superior ability to recognize and eliminate PD-$L1^+$ tumor cells in different tumor types.

Given the engineered release of IL15 and NKG2A-scFv by ^{ex}PD1-NK cells, we next investigated their contribution to sustaining the anti-tumor activity over 72 hours of co-cultures with tumor cells. This timeframe is sufficient to allow the activity of both molecules. Using live-cell imaging to monitor tumor cell viability, we found that ^{ex}PD1-NK cells significantly inhibited tumor cell proliferation and induced early Caspase 3/7 activation in PD-$L1^+$ SK-N-AS neuroblastoma cells compared to mock-NK cells (Fig. 4e, f and Movies S1–S3). A similar, though less pronounced, effect was observed in PD-$L1^-$ IMR-32 neuroblastoma cells (Fig. 4e, f, and Movies S4–S6). These results suggest that IL15 release could promote NK cell survival, while the NKG2A-scFv prevents HLA-E/NKG2A inhibitory interaction, thereby maintaining the cytotoxic effect over time and acquiring the ability to target PD-L1-expressing tumors.

To better recapitulate spatial tumor-immune interactions within the TME, we assessed ^{ex}PD1-NK cell cytotoxicity in a 3D organoid model using organoids (PDOs) from pancreatic cancer patients. Following disaggregation and Matrigel embedding, organoids were cultured for 3 days before the addition of mock- or ^{ex}PD1-NK cells. Organoid growth was then monitored over 72 hours. As shown in Fig. 4g, while PDOs alone expanded in size, those co-cultured with ^{ex}PD1-NK cells significantly limited their growth, whereas mock-NK cells had a reduced effect (Movies S7–S9 and Supplementary Fig. 5a). Although PD-L1 expression in PDOs was low, the enhanced anti-tumor activity of ^{ex}PD1-NK cells could be due to their ability to circumvent HLA-E-mediated inhibition. Moreover, we observed upregulation of PD-L1 on the PDO surface after co-culture with NK cells (Fig. 4h and Supplementary Fig. 5b). These findings suggest that ^{ex}PD1-NK cells may be beneficial for a wide range of tumors, expressing or not PD-L1.

^{ex}PD1-NK cells counteract hematological and solid tumor growth in vivo

To assess the in vivo therapeutic efficacy of ^{ex}PD1-NK cells, immunodeficient NSG mice were engrafted with FireFly/GFP (FF/GFP) NALM-18 leukemia cells (day -3). After tumor engraftment (day 0), mice were adoptively infused intravenously (i.v.) with one dose of ^{ex}PD1- or mock-NK cells. Untreated mice were used only to monitor tumor growth. Mice were monitored over time, and tumor progression was analyzed by in vivo bioluminescence scanning on days 7, 14, and 21 (Supplementary Fig. 6a). Tumor burden, as measured by the increase in bioluminescence intensity, rose rapidly in both untreated and mock-NK cell-treated mice. In contrast, ^{ex}PD1-NK cell-treated mice exhibited suppression of tumor growth, maintaining a markedly lower bioluminescence signal throughout the 21 days (Fig. 5a, b). Regarding the leukemia in vivo model, we evaluated tumor progression based on dynamic growth parameters. Specifically, a ≥ 5-fold increase in bioluminescence signal within one week was considered a critical threshold indicative of aggressive tumor expansion. As shown in Fig. 5b, mice treated with ^{ex}PD1-NK cells displayed higher event-free survival compared to mock-NK cell-treated and untreated mice. Flow cytometric analysis of residual tumor cells, identified as GFP-positive cells, at the study endpoint (day 21) further confirmed these findings. Thus, the absolute number of GFP^+-tumor cells in the BM was high in both untreated and mock-NK cell-treated mice. In contrast, it was significantly reduced in ^{ex}PD1-NK cell-treated mice, providing further evidence of anti-tumor activity of ^{ex}PD1-NK cells (Fig. 5c). Importantly, only ^{ex}PD1-NK cells were detectable in both spleen and bone marrow, while in mock-NK cell-treated mice, NK cells were undetectable (Fig. 5d).

To assess the in vivo therapeutic efficacy of ^{ex}PD1-NK cells in a solid tumor setting, immunodeficient NSG mice were subcutaneously or orthotopically engrafted with FF/GFP SK-N-AS human neuroblastoma tumor cells on day -3. SK-N-AS cells represent one of the most immunosuppressive and NK-resistant neuroblastoma models, providing an ideal "worst-case" scenario to evaluate the effectiveness of ^{ex}PD1-NK cells.

Following tumor establishment (day 0), mice received an i.v. infusion of ^{ex}PD1-NK cells or mock-NK cells. Untreated mice served only as negative controls. Tumor progression was monitored longitudinally using in vivo bioluminescence imaging for the orthotopically tumor model or caliper measurements on days 7,

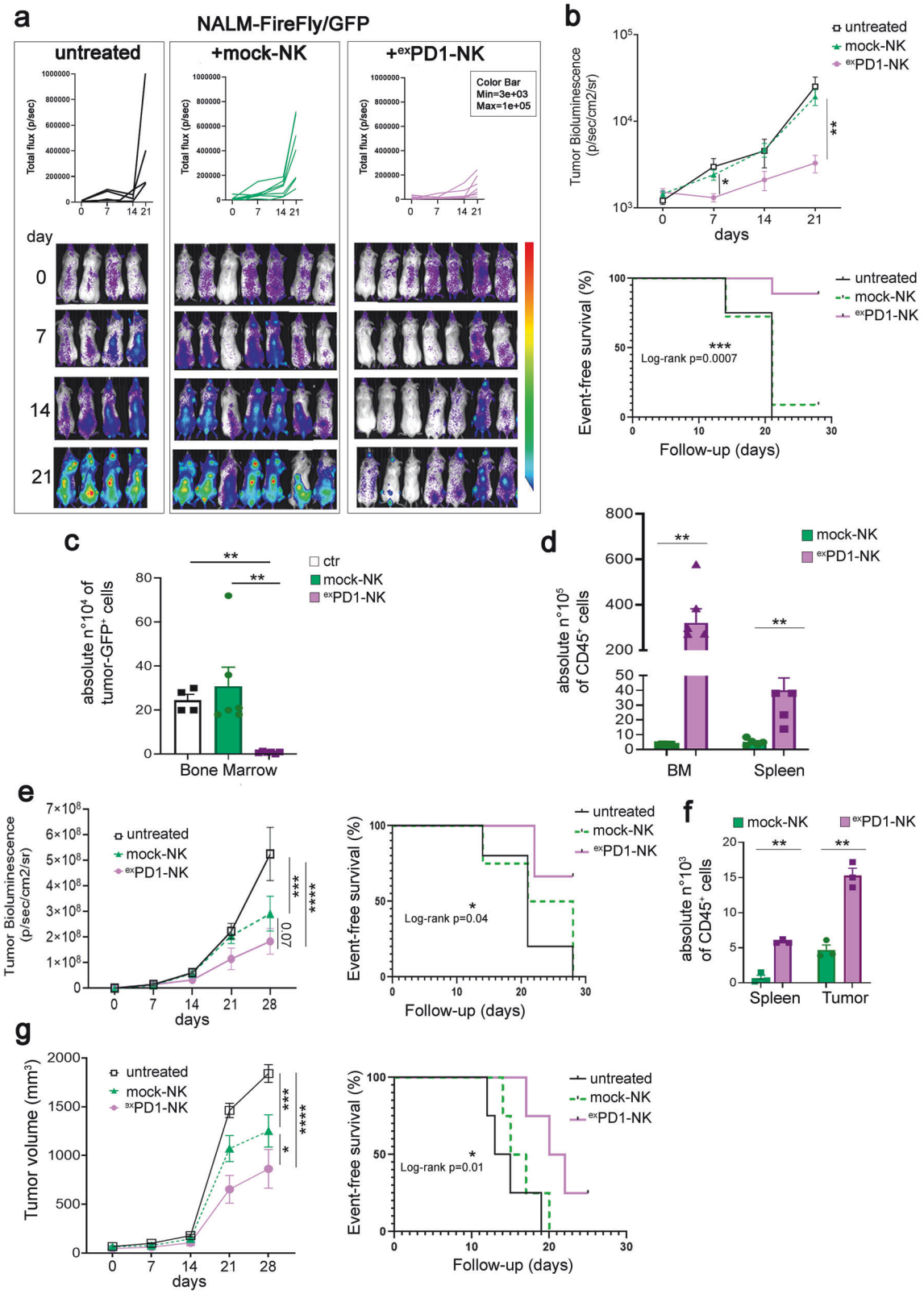

14, 21, and 28 post-treatment for the subcutaneously tumor model. The bioluminescence signal (Fig. 5e and Supplementary Fig. 6b) in orthotopic tumor-engrafted mice and the tumor volume in mice injected subcutaneously (Fig. 5g) increased progressively in both the untreated and mock-NK cell-treated groups. In contrast, mice treated with ^{ex}PD1-NK cells exhibited significantly delayed tumor growth, with reductions in tumor volume and bioluminescence signal throughout the study period. We also assessed event-free survival in the orthotopic model using bioluminescence imaging. A threshold of a 10-fold increase in

Fig. 5 ^{ex}PD1-NK cells displayed in vivo high anti-tumor activity and persistence. **a** Quantification of bioluminescence and representative image series evaluated at the indicated time points of a single mouse engrafted with NALM-FF/GFP. Tumor-transplanted mice were untreated ($n = 4$) or treated with mock- ($n = 7$) or ^{ex}PD1-NK (n = 7) cells. **b** Upper panel shows mean ± SEM of tumor bioluminescence kinetics (photons per second per square centimeter per steradian) in untreated, mock- or ^{ex}PD1-NK cells treated mice. *p*-values were calculated using the 2-way ANOVA test for multiple comparison (*$p < 0.05$ and **$p < 0.01$). Lower panel shows Event-Free Survival between the 3 different groups. *p*-value was calculated as the Log-rank test. **c** Absolute number ± SEM of GFP$^+$ tumor cells in the BM of mice at day 21 after administration of effector cells: ctr (white bar, $n = 4$), mock- (green bar, $n = 6$), or ^{ex}PD1-NK (pink bar, $n = 6$) cells. *p*-values were calculated using the Mann-Whitney t-test (**$p < 0.01$). **d** Absolute number ± SEM of GFP$^-$/hCD45$^+$ cells in the BM and spleen of mice at day 21 after administration of effector cells: mock- (green bars) or ^{ex}PD1-NK (pink bars) cells. *p*-values were calculated using the Mann-Whitney t-test (**$p < 0.01$). **e** Left panel shows mean ± SEM of tumor bioluminescence kinetics (photons per second per square centimeter per steradian) evaluated at the indicated time points of a mouse orthotopically (adrenal gland) engrafted with SK-N-AS FF/GFP. Tumor-transplanted mice were untreated ($n = 3$) or treated with mock- ($n = 3$) or ^{ex}PD1-NK ($n = 3$) cells. *p*-values were calculated using the 2-way ANOVA test for multiple comparison (***$p < 0.001$, and ****$p < 0.0001$). The right panel shows Event-Free Survival between the 3 different groups. *p*-value was calculated as the Log-rank test. **f** Absolute number ± SEM of GFP$^-$/hCD45$^+$ cells in the spleen and tumor at the clinical endpoint, when mice had to be sacrificed. *p*-values were calculated using the Mann-Whitney t-test (**$p < 0.01$). **g** Left panel shows the mean ± SEM of tumor volume (mm^3) evaluated at the indicated time points of a mouse subcutaneously engrafted with SK-N-AS-FF/GFP. Tumor-transplanted mice were untreated ($n = 4$) or treated with mock- (n = 4) or ^{ex}PD1-NK (n = 4) cells. *p*-values were calculated using the 2-way ANOVA test for multiple comparison (*$p < 0.05$, ***$p < 0.001$, and ****$p < 0.0001$). The right panel shows Event-Free Survival between the 3 different groups. *p*-value was calculated as the Log-rank test

bioluminescence signal relative to the baseline (time zero) was established as a critical parameter to assess tumor growth and to determine experimental endpoints in accordance with ethical guidelines (Fig. 5e). Similarly, in subcutaneous tumor models, mice were considered for euthanasia when tumor size exceeded 1,000 mm^3, or earlier if signs of ulceration, impaired mobility, or systemic distress were observed (Fig. 5g).

At the study endpoint, flow cytometric analysis showed a higher abundance of human ^{ex}PD1-NK cells within the spleen and the excised tumor of ^{ex}PD1-NK cell-treated mice compared with mice treated with mock-NK cells, indicating both enhanced tumor infiltration and presence (Fig. 5f and Supplementary Fig. 6c).

Similar results were obtained by using Group 3 Medulloblastoma (MB) cells in vitro and in vivo. ^{ex}PD1-NK cells controlled the growth and efficiently killed Group 3 MB (D283-Med and D341-Med) spheroids (3D cultures) at different E:T ratios as compared to mock-NK cells (Supplementary Fig. 5d, e). We further assessed the activity of ^{ex}PD1-NK cells in an orthotopic MB mice model intracranially injected with FF/GFP-D283-Med tumor cells. Of note, as previously described,[38] to enhance NK cell activity, recombinant (r) IL15 was administered intravenously only to the mock-NK cell group. In contrast, ^{ex}PD1-NK cells were injected alone because they were able to produce IL15. In this setting, only ^{ex}PD1-NK cells displayed a partial control of tumor growth (Supplementary Fig. 6f, g).

Furthermore, to assess the potential systemic toxicity of ^{ex}PD1-NK cell treatment, we performed longitudinal body weight and serum biochemical analyses in tumor-bearing mice at two independent time points. The first assessment was performed 1 day after NK cell infusion (for both mock and ^{ex}PD1-NK cells) to assess acute toxicity, and the second at the end of the experiment to assess chronic toxicity. The serum analysis revealed no evidence of liver injury, cholestatic dysfunction, renal impairment, or systemic organ compromise linked to the NK cell treatment (Supplementary Fig. 7a). Notably, lactate dehydrogenase (LDH), a marker of tissue damage and tumor burden, was elevated at baseline across all three groups but showed a significant decrease, particularly in animals receiving NK cells and even more markedly in those treated with ^{ex}PD1-NK cells, consistent with reduced tumor-associated tissue damage. We additionally performed hematoxylin-eosin (H&E) staining of the spleen across the different experimental groups (Supplementary Fig. 7b).

Similar splenic architecture was detected in tumor-bearing mice, regardless of whether they were untreated or treated with mock- or ^{ex}PD1-NK cells. These results demonstrate the safety of treatment with NK cells, including ^{ex}PD1-NK cells, despite their engineering with multiple components. Therefore, the ^{ex}PD1-NK cell platform appears to be a promising and safe approach for enhancing immune cell-based therapies.

^{ex}PD1-NK cells improve their metabolic fitness and migratory capacity after tumor interaction

To further characterize the functional properties of ^{ex}PD1-NK cells, we performed high-dimensional phenotypic profiling by analyzing over 350 surface markers both before and after 24 hours of co-culture with a neuroblastoma tumor cell line. A comparative analysis of mock- and ^{ex}PD1-NK cells showed that the levels of most surface molecules, including activating and inhibitory NK cell receptors, as well as exhaustion markers, were not significantly altered in both NK cells before and after co-culture with tumor cells (Supplementary Figs. 8 and 9).

Conversely, ^{ex}PD1-NK cells in basal conditions expressed higher levels of CD110, CD81, CD279, CD244; CD38, CD29, CD44, CD2, CD48, CD147, CD45RA, CD55, CD43, and CD99 compared to mock-NK cells (Fig. 6a). After exposure to neuroblastoma tumor cells, ^{ex}PD1-NK cells exhibited upregulation of CD148, CD53, CD45RB, CD69, CD26, and CD31 (Fig. 6d). These molecules are involved in various immune processes, including lymphocyte activation, cell adhesion and migration (Fig. 6b, e), suggesting a potential capability of ^{ex}PD1-NK cells to infiltrate tissues.

We then analyzed the expression of the ligands corresponding to the proteins upregulated by ^{ex}PD1-NK cells in "hot" and "cold" tumors. Their expression was higher in hot tumors than in cold tumors, revealing a correlation with immune infiltration status (Fig. 6c, f). However, these ligands were also observed in cold tumors as well, suggesting an enhanced ability of ^{ex}PD1-NK cells to effectively act in tumors typically characterized by low immune infiltration.

To further investigate the potential clinical relevance of ^{ex}PD1-NK cells, we performed a survival analysis for tumor-expressed ligands associated with up-regulated ^{ex}PD1-NK cell surface markers across different tumor types. Notably, some tumor patients with low expression of these ligands showed significantly poorer overall survival compared to those with high ligand expression (Fig. 6g). This observation may have important therapeutic implications: ^{ex}PD1-NK cells could be recruited by tumors that naturally express high levels of these ligands. At the same time, given the increased expression of the corresponding receptors on ^{ex}PD1-NK cells, tumors with low ligand expression may still be effectively targeted.

A key goal of adoptive immunotherapy is to maintain the metabolic state of immune cells. Thus, we assessed the metabolic fitness of ^{ex}PD1-NK cells by profiling their metabolic and bioenergetic status before and after co-culture with neuroblastoma (SK-N-AS) tumor cells. Under both basal and stress conditions, ^{ex}PD1- and mock-NK cells exhibited comparable

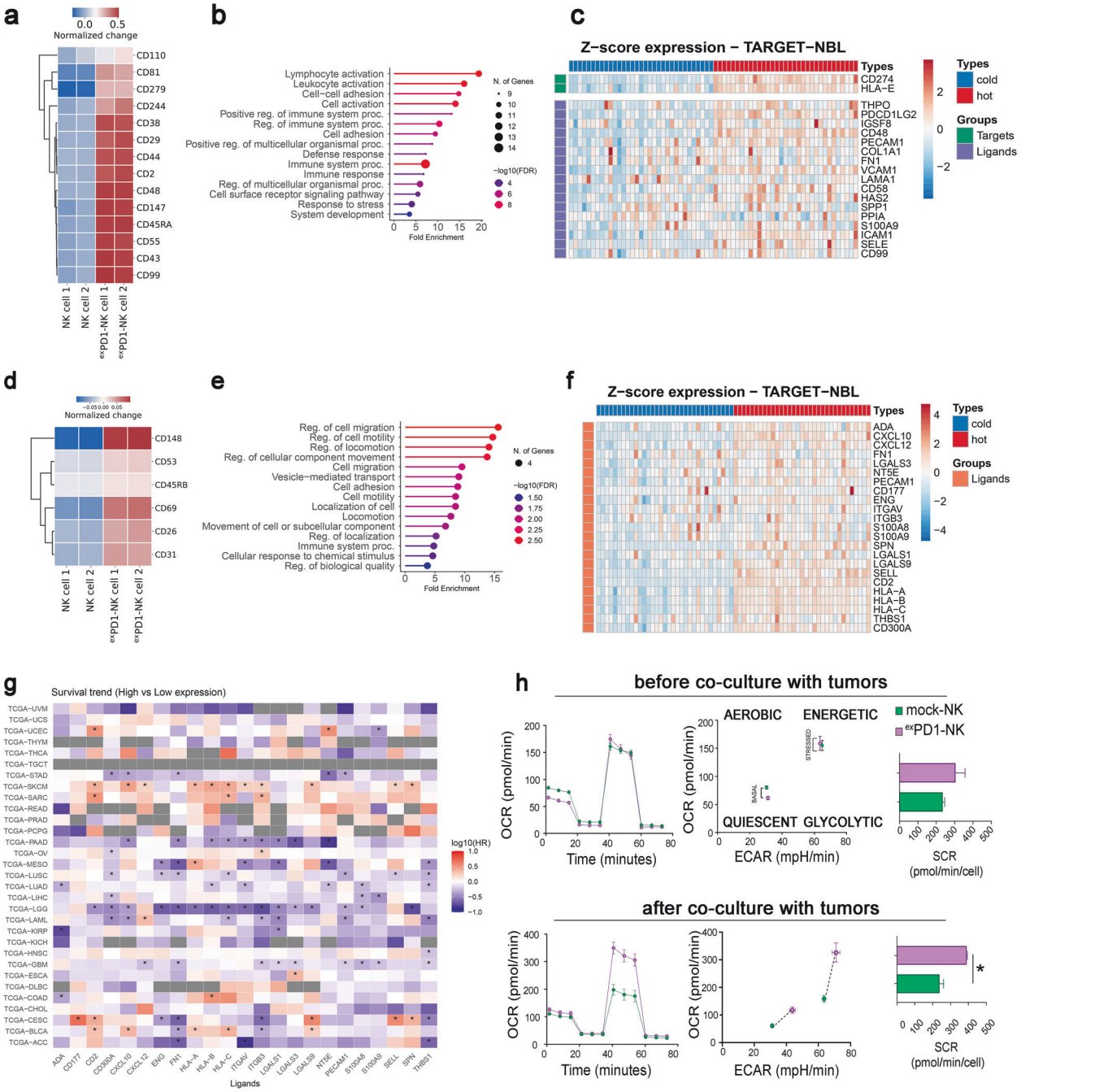

Fig. 6 Phenotypic profiling reveals upregulation of immune activation, migration, and adhesion markers in ^{ex}PD1-NK cells. **a**. Significantly differentially expressed surface markers in ^{ex}PD1-NK cells compared to mock-NK cells, identified via high-dimensional phenotypic profiling. Paired two-tailed Student's t-test ($p \leq 0.05$) was used for statistical significance. **b** Gene Ontology (GO) analysis of biological processes enriched among genes upregulated in ^{ex}PD1-NK cells. **c** Heatmap showing expression levels of PD-L1, HLA-E, and tumor cell ligands corresponding to proteins encoded by genes upregulated in ^{ex}PD1-NK cells, across "hot" and "cold" NBL tumor samples. Significantly differentially expressed surface markers (**d**), GO (**e**), and heatmap (**f**) as in (**a**–**c**) in ^{ex}PD1-NK cells compared to mock-NK cells after tumor contact. **g** Heatmap of hazard ratios of tumor ligands in (**f**), across different tumor types. Blue boxes indicate tumors where low ligand expression is linked to poorer survival, while red boxes indicate tumors where high ligand expression corresponds to worse outcomes. Asterisks identify statistically significant differences in the overall survival between groups with high or low expression of the indicated ligands. **h** Metabolic profiling of ^{ex}PD1- (pink) and mock-NK (green) cells before and after 24-hour co-culture with tumor cells. Oxygen consumption rate (OCR), energetic map, and spare respiratory capacity (SRC). Paired two-tailed Student's *t*-test, ($p \leq 0.05$) was used

extracellular acidification rates (ECAR) and oxygen consumption rates (OCR) (Fig. 6h). However, after 24 hours of co-culture with SK-N-AS tumor cells, ^{ex}PD1-NK cells displayed significantly higher metabolic activity under stress conditions, characterized by increased OCR and spare respiratory capacity (SRC) than co-cultured mock-NK cells (Fig. 6h). These findings suggest that ^{ex}PD1-NK cells possess superior metabolic adaptability and bioenergetic reserves, which may render them more capable of responding to increased energetic demands and stress following interaction with tumor cells.

DISCUSSION

The fight against tumors demands major efforts, as it requires defeating the tumor and counteracting the effect of the TME that strongly reduces the effectiveness of immune responses and treatments.

Current therapies target specific antigens on tumor cells, but these antigens may be rare, or their expression may become deregulated during tumor progression and metastasis.[39] A promising strategy is to focus on "common" antigens shared by different tumors, such as those functioning as immune checkpoint inhibitors or immunosuppressive molecules. In particular, tumors frequently exploit surface immune checkpoint molecules, such as PD-L1 and HLA-E, to escape NK and T cell-mediated surveillance.[40]

This study proposes a novel and efficient approach to enhance the effectiveness of NK cell-based immunotherapy, which may provide an important basis for current cancer treatments.[41] Indeed, we developed a multi-faceted preclinical study that underscores not only the clinical relevance of PD-L1 and HLA-E as immune evasion markers but also introduces a rationally designed first-in-class, multifunctional NK cell engineering strategy that effectively neutralizes different suppressive cues. Our pan-cancer transcriptomic analyses show that PD-L1 and HLA-E are consistently upregulated across diverse tumor types in both adult and pediatric hematological and solid tumors. Notably, their expression was positively correlated with markers of immune infiltration. This suggests that tumors can upregulate ligands involved in immune infiltration in response to interferon-mediated inflammation, effectively protecting tumor cells from immune effector cell attack[42] despite their appearance as immunologically "hot".[31] These findings are in line with prior reports highlighting the paradox of tumors that, although infiltrated by immune cells, are resistant to therapy with immune checkpoint inhibitors due to redundant suppressive circuits.[43] Importantly, the consistent co-expression of PD-L1 and HLA-E highlights their value as biomarkers of immune evasion and indicates the need to target both of them in combinatory immunotherapy, particularly in the context of innate immune effector cell therapy.

We have developed a protocol to produce large numbers of ready-to-use cellular products using donor-derived, allogeneic, genetically modified, and mature NK cells. These cells express an innovative activating chimeric receptor that abolishes and reverts PD-L1-negative signals. In addition, they disrupt HLA-E-mediated suppression and support NK cell survival by secreting IL15. This integrated design effectively overcomes multiple, non-redundant immunosuppressive pathways of the tumor, using a tri-cistronic single vector suitable for clinical-grade cell manufacturing.

Importantly, the tri-cistronic vector enables precise regulation of the functional contribution of each module. Notably, separate analyses of the individual vector components show that the simultaneous presence of all elements is crucial, as only their coordinated, synergistic activity ensures optimal functionality while preserving safety.

These findings indicate that the complete tri-cistronic construct is crucial for enhancing the antitumor efficacy and survival capacity of genetically engineered ^{ex}PD1-NK cells. This approach aligns with recent efforts to combine checkpoint blockade with cytokine support.[44,45] We also show that ^{ex}PD1-NK cells not only retain their cytotoxic function and native receptor repertoire following transduction but also exhibit enhanced killing of PD-L1^{+} and HLA-E^{+} tumor cells both in 2D co-cultures and 3D patient-derived tumor organoids. Importantly, these effects were observed regardless of the tumor origin (both hematologic and solid), highlighting the broad applicability of our platform. The secreted NKG2A-scFv successfully disrupted the inhibitory interaction between NKG2A and HLA-E, an upregulated axis in many tumors, associated with NK cell dysfunction.[46] Importantly, scFvs are characterized by a much shorter half-life compared to full-length antibodies. In this regard, our platform builds on the success of anti-NKG2A monoclonal antibodies (e.g., Monalizumab), introducing the added benefit of localized, autocrine blockade within the tumor site, which may potentially minimize systemic toxicities.[47]

Notably, ^{ex}PD1-NK cells displayed enhanced metabolic adaptability and elevated spare respiratory capacity upon tumor engagement. These characteristics are critical for sustained NK cell activity in nutrient-depleted, immunosuppressive tumor niches.[48,49] Unlike T cells, which often undergo exhaustion,[50] NK cells rely on metabolic flexibility and rapid adaptability, exploiting IL15 not only for their proliferation but also as a protective cytokine.[51] By integrating IL15 directly into our vector, we support ^{ex}PD1-NK cells through both functional and environmental stressors, ensuring their maintenance and cytolytic capacity even in hostile tumor settings. Indeed, the in vivo efficacy of ^{ex}PD1-NK cells was prominent since a single dose resulted in durable tumor control and prolonged NK cell presence in both the spleen and tumor of leukemia-, neuroblastoma-, and medulloblastoma-bearing mice.

These outcomes mirror the best results obtained from engineered CAR-NK cell therapies,[28] but with the added advantage of targeting immune evasion rather than tumor-associated antigens alone, which may reduce the likelihood of tumor escape via antigen loss. It is known that immune cells, particularly NK cells, may exert their anti-tumor activity by releasing pro-inflammatory cytokines, including IFN-γ, which promotes tumor immune evasion through PD-L1 expression.[52,53] However, this process, in our setting, facilitates the engagement of ^{ex}PD1-NK cells. This effect is further supported by autocrine IL15, which allows NK cell prolonged survival, and by the interruption of the NKG2A/HLA-E axis by soluble NKG2A-scFv.

Another important feature of these new engineered NK cells is the upregulation of molecules involved in different immune cell activation, migration, and adhesion processes. Notably, the ligands corresponding to these molecules are found in all tumors, regardless of their levels of immune infiltration, whether categorized as "hot" or "cold." This suggests that ^{ex}PD1-NK cells may have the ability to infiltrate tumors that typically limit immune infiltration. Survival analyses of tumor patients revealed that the low expression of some tumor ligands could be linked to poor prognosis in different tumor types. Since ^{ex}PD1-NK cells, upon tumor interaction, express high levels of the activating receptors corresponding to these ligands, this suggests that ^{ex}PD1-NK cells may have an increased ability to recognize and kill tumors, offering a promising strategy to improve patient outcomes.

Our platform was evaluated in a stringent allogeneic model, utilizing HD-derived NK cells, which highlights its clinical feasibility for off-the-shelf applications. Notably, NK cell-based therapy holds a distinct advantage over T cell-based therapies related to its derivation from allogeneic donors, which limits the risk of graft-versus-host disease (GvHD) and enables broader and faster application in acutely ill tumor patients. This is particularly relevant for high-risk or refractory pediatric and adult tumor patients, i.e., patients for whom time-sensitive, pre-manufactured solutions with standardized cell numbers represent a great advantage. In addition, the enhanced proliferation, viability, and long-term persistence of ^{ex}PD1-NK cells in vivo further support their usefulness as a durable and scalable therapeutic product. Furthermore, unlike T cells, which require individualized production or complex HLA matching, our NK cell platform offers universal pre-armed immune effector cells.

In conclusion, our study introduces a novel NK cell-based immunotherapy platform that addresses key limitations of the current strategies, including immune checkpoint redundancy, metabolic suppression, and poor persistence. By simultaneously targeting PD-L1 and HLA-E, and by equipping NK cells with autonomous IL15 support, we provide a versatile and potent

therapeutic framework for aggressive cancers, particularly in the allogeneic setting. In a therapeutic landscape increasingly driven by the search for precision and adaptability, ^{ex}PD1-NK cells may represent a timely and transformative approach for patients in urgent need of effective, off-the-shelf solutions. This new therapeutic strategy provides a proof-of-concept for developing innovative cancer immunotherapies that can overcome the hurdles currently present in non-allogeneic settings, as well as those driven by tumor-mediated immunosuppression and the tumor's ability to adapt and evade immune system recognition. Importantly, due to the diverse composition and related inhibitory mechanisms present in different tumors, the effectiveness and potential adaptability of this new platform may offer a valuable proof of concept for targeting various tumor types through genetically engineered NK cells.

MATERIALS AND METHODS

NK cell isolation and expansion

Peripheral blood mononuclear cells (PBMC) were obtained from healthy donors (HD) buffy coat from the transfusion center of IRCCS Bambino Gesù Children's Hospital, Rome (Approval of Ethical Committee prot. N° 729) and isolated after density gradient centrifugation (Ficoll-Lympholyte, Cederlane). NK cells were purified using NK isolation kit II (Miltenyi Biotec) or Rosettsep 10 (StemCell) and shortly activated (72 h) with IL15 (150U/ml, Miltenyi Biotec), IL2 (50U/ml), and IL1β (2000U/ml, Miltenyi Biotec) in NK MACS medium (Miltenyi Biotec) supplemented with 5% human serum and 2 mM Glutamax. Purity was evaluated by flow cytometry; only >96% of purity was considered suitable for cultures. Cells were maintained in a humidified atmosphere containing 8% CO_2 at 37 °C.

Generation of γ-retroviral vector and NK cell transduction

A γ-retroviral vector was constructed to encode a chimeric construct comprising PD1-NKG2D.4-1BB.2 A.NKG2A(scFv).2A.IL15. This tri-cistronic vector enables the expression of a transmembrane fusion receptor containing the PD-1 ectodomain, designed to bind PD-1 ligands, fused in-frame with a secretable scFv targeting NKG2A and the cytokine IL15.

To validate the contribution of each engineered component of our γ-retroviral vector, we generated three new tri-cistronic vectors by selectively replacing individual components while retaining the same backbone and expression configuration. We developed tri-cistronic vectors in which the NKG2A-scFv or IL15 transgenes, or both, were replaced with an irrelevant protein (IP), referred to as w/o-NKG2A, w/o-IL15, or w/o-NKG2A/IL15. IP for NKG2A-scFv was ΔCD19, while for IL15 was red fluorescent protein (RFP). These modifications preserved the overall architecture of the vectors while specifically removing NKG2A and/or IL15 from the system.

Retroviral supernatant was produced by transient transfection of HEK-293T cells as described previously,[54,55] and viral titers were quantified using the Retro-X™ qRT-PCR Titration Kit (Takara Bio). Human NK cells were cultured in expansion medium for 3 days before transduction, then seeded into the RetroNectin-coated plates (Takara Bio, Japan) containing the spin-inoculated viral supernatant. The culture medium was replaced after 72 hours with NK MACS Medium plus 5% human serum and 2 mM Glutamax with IL15 (150U/ml, Miltenyi Biotec) and IL2 (50U/ml). Transduction efficiency was assessed by flow cytometry.

Cell lines and cultures

The NALM-18 (Childhood B acute lymphoblastic leukemia), Karpas (human lymphoma), HL-60 (acute promyelocytic leukemia), HLA-E$^+$ LCL 721.221.G tumor cells, HEK-293T, and THP-1 (acute monocytic leukemia) cancer cell line were kindly provided by Dr Pende D. (IRCCS, Policlinico San Martino, Genoa, Italy) and cultured in RPMI 1640 (Euroclone, Milan, Italy) supplemented with 10% FBS (Euroclone), 1% penicillin/streptomycin (Euroclone), and 1% L-glutamine (Euroclone). SKNAS, SKNSH, IMR32, and SHSY5Y neuroblastoma cell lines (ATCC) were cultured in Dulbecco's modified Eagle's (DMEM) supplemented with 10% FBS, 1% penicillin/streptomycin, and 1% L-glutamine. D283-Med and D341-Med cells were obtained from the American Type Culture Collection (ATCC). Cell lines were grown in MEM supplemented with 20% of Fetal Bovine Serum (FBS), 1% of MEM Non-Essential Amino Acids (NEAA), 1% of Sodium pyruvate, and 1% of PenStrep. All cell lines were cultured in a humidified atmosphere with 5% CO_2 at 37 °C. For the generation of eGFP-Firefly-Luciferase (FF/GFP) cell lines, the retroviral vector encoding eGFP-Firefly-Luciferase was used in selected experiments to label positive (PD-L1$^+$) or negative (PD-L1$^-$) tumor cells. Cells were maintained in a humidified atmosphere containing 5% CO_2 at 37°C. All cell lines were routinely 15 tested for mycoplasma and surface expression of target antigens.

Protein purification and characterization

The anti-NKG2A scFv was purified from the conditioned media of HEK-293T mammalian cells expressing proteins using affinity columns and characterized. Particularly, the scFv was purified on a Pierce Protein L Plus Agarose column (Thermoscientific) according to the manufacturer's instructions. scFv was dialyzed against phosphate buffer saline (PBS) overnight at +4 °C and sterile filtered using a Millex-GP 0.22 µm filter unit (Millipore). Subsequently, it was analyzed by sodium dodecyl sulfate-polyacrylamide gel electrophoresis (SDS-PAGE) using NuPAGE Novex Bis-Tris gel (Thermo Scientific) under reducing conditions.

Detection of IL15 by ELISA assay

HEK-293T cells, ^{ex}PD1- and mock-NK cells were cultured for different time points and cellular concentration in media containing 10% FBS, 1% Pen/Strep, and 2 mM Glutamax. Levels of IL15were measured using IL15 human ELISA kits (R&D Systems, DY247-05). All procedures were performed as described in the manufacturer's instructions.

Immunoblotting

For the evaluation of protein levels, the cell pellet was lysed in RIPA buffer supplemented with protease and phosphatase inhibitors, then incubated on ice for 20 minutes. Cell lysates were centrifuged at 15,000 g for 15 minutes to remove insoluble components. The supernatants were collected, and proteins were quantified using the Bradford assay (Bio-Rad). Cell lysate was heated at 85 °C for 2 min in 4X Bolt™ LDS Sample Buffer (Invitrogen) and loaded on precast Bolt 4–12% Bis-Tris Plus Gels (Invitrogen). After electrophoresis, proteins were transferred to a nitrocellulose membrane (Amersham, GE Healthcare). The membranes were blocked in 5% nonfat dry milk (Cell Signaling Technology) in PBST (PBS containing 0.05% Tween 20) for one hour at room temperature (RT) and then incubated overnight at 4 °C with the following primary antibodies: Anti-p-JNK (Cell Signaling Technology #mAb 9251S), Anti-p-cJun (Cell Signaling Technology #mAb 91952), Anti-p-NFkB (Cell Signaling Technology #mAb 3033S), and Anti-β-Actin (Sigma-Aldrich A5441). Following 1-hour incubation with HRP-conjugated secondary antibodies (Cell Signaling Technology goat anti-rabbit IgG #7074 and goat-anti-mouse IgG #7076S), the signal was detected using ECL Prime Western Blotting Detection Reagent (Amersham, GE Healthcare) on a Uvitec Cambridge Mini HD9.

Monoclonal antibodies and cytofluorimetric analysis

For cytofluorimetric analysis, cells were stained with surface antibodies in PBS containing 5% FCS for 20 min at 4 °C. Expression of cell surface molecules was determined by flow-cytometry using standard methodology. The following mAbs were used: CD3-APC

(clone REA613 | SK7, Miltenyi Biotec), CD19-Fitc (clone LT19, Miltenyi Biotec), PD-1-PE ((clone PD1.3.1.3, Miltenyi Biotec), NKG2D-PE/DAZZLE (clone 1D11, Biolegend), DNAM1-PC7 (clone 11A8, Biolegend), NKp44-APC (clone P44-8, Biolegend), CD45-APC700 (clone H130, Biolegend), CD57-PB (clone HNK-1, Biolegend), CD56-PC7 (clone N901, Beckman Coulter), CD56-BV650 (clone NCAM16.2, BD), NKG2A-APC (Z199, Beckman Coulter), CD94-FITC (DX22,BioLegend), PD-L1-PECF594 (clone MIH1, BD), PD-L2-PEVio615 (clone REA985 | MIH18, Miltenyi Biotec), HLA-E-PE (clone 3D12, BD), Macs Marker Screen V2 (Miltenyi Biotec). For the proliferation assays, HD-NK cells were labeled with CellTrace™ CFSE Cell Proliferation Kit (Invitrogen, #C34554) following the manufacturer's instructions and resuspended in RPMI1640 containing 10% FBS, 1% Pen/Strep, and 2 mM Glutamax. CFSE-HD-NK cells were co-cultured in transwell conditions with genetically modified NK cells. At day 7, HD-NK cells (bottom wells) were harvested and analyzed by flow cytometry. In selected co-culture experiments, an anti-IL15 mAb was added (Bio-Techne, #MAB247, 5ug/ml). Samples were analyzed on a Cytoflex S and Cytoflex LX (Beckman Coulter). Data were analyzed using Cytexpert (Beckman Coulter) and FlowJo 10 software (BD Biosciences). For each sample, we analyzed a minimum of 50,000 events.

Cytotoxic assay

The cytotoxic assay was performed as previously described[56] using as a medium: RPMI1640 containing 10% FBS, 1% Pen/Strep, and 2 mM Glutamax. Briefly, target cells were either labeled with Green Cell Tracker (CMFDA; Invitrogen, Thermo Fisher Scientific) according to the manufacturer's instructions or directly used target cells transduced with the eGFP-Firefly-Luciferase vector. Target cells were incubated with NK cells at different effector/target (E:T) ratios. After 4 hours (h) of incubation at 37°C, propidium iodide (PI, Sigma-Aldrich) was added to detect dead tumor cells. Cells were acquired with the Beckman-Coulter Cytoflex-S/LX flow cytometer, and live target cells were identified as $CMFDA^+$ PI^- or GFP^+ PI^-, whereas dead target cells were $CMFDA^+$ PI^+ or GFP^+ PI^+. The percentage of cell lysis was calculated as follows: % cell lysis = ((% of dead cells cultured with NK)−(% of spontaneous lysis)) / (100 − % of spontaneous lysis) × 100. For long-time (48 h) co-culture experiments, ^{ex}PD1- and mock-NK cells were co-cultured at a 4:1, 1:1, or 1:4 E:T ratio with tumor cells. Following 2 days of incubation at 37°C, residual tumor cells and NK cells were evaluated by flow-cytometry analysis.

Seahorse extracellular flux analysis

Seahorse experiments were performed on isolated NK cells using the XF Cell Mito Stress kit (Seahorse Bioscience). OCR and ECAR were measured with XF96 Extracellular Flux Analyzers (Seahorse Bioscience). Briefly, NK cells were plated on poly-d-lysine-coated 96-well polystyrene Seahorse plates (50 000 NK cells/well), equilibrated for 1 hour at 37 °C, and assayed for OCR (pmol/min) and ECAR (mpH/min) in basal conditions and after addition of oligomycin (1 μM), carbonyl cyanide-4-phenylhydrazone (1.5 μM), and antimycin A/rotenone (1 μM/0.1 μM). All of the SeaHorse experiments were performed using the manufacturer's recommended media (pH 7.4), without phenol red, to standardize the pH conditions in all samples.

Real-time tumor cell cytotoxicity assays

To discriminate tumor and NK cells in co-culture, SK-N-AS and IMR-32 cells were transduced with a nuclear-restricted near-IR fluorescent label following the manufacturer's instructions (Sartorius). Target tumor cells were seeded in 96-well flat-bottom plates. After overnight incubation, Caspase -3/7 Green Dye (Sartorius) and effector cells were added to the medium. Tumor and NK cells were co-cultured at a 1:1 E: T ratio for 72 h in the Incucyte Live-Cell Analysis System. The assay plate scan will be scheduled every 4 hours. Tumor cells will be counted with the IncuCyte SX5 Live-Cell Analysis System every time scanned to monitor tumor growth.

3D human pancreatic PDO culture

Patient-derived organoids were kindly provided by Prof. Dr. MD. Maximilian Reichert (Technical University of Munich (TUM), Germany. PDO were growth in Matrigel (Corning) domes in 24-well plates in feeding media contained the following components: AdDMEM/F12 medium supplemented GlutaMax (1X, Life Technologies), B27 (1X, Life Technologies), Primocin (100 μg/mL, InvivoGen), N-acetyl-L-cysteine (1.25 mM, Sigma-Aldrich), Nicotinamide (10 mM, Sigma-Aldrich), recombinant human Wnt3a protein (100 ng/mL, R&D Systems), mNoggin (100 ng/mL, Preprotech), EGF (50 ng/mL, Life Technologies), Gastrin (10 nM, Sigma-Aldrich), FGF10 (100 ng/mL, Preprotech), and A83- 01 (0.5 μM, Tocris). For organoids passing, the feeding medium was aspirated, and cold PBS was added to the well to dissolve the Matrigel matrix. Then, the mixture of organoid, Matrigel, and PBS was transferred into a 15 ml tube and centrifuged. The organoid pellet was dissociated by enzymatic digestion for 5 to 10 minutes with TrypLE (Life Technologies) at 37 °C. After dissociation, the organoids were washed with cold PBS, mixed with Matrigel, and plated in a prewarmed 24-well plate.

Spheroids of MB cells

To assess the impact of tumor architecture, GFP^+D283-Med and D341-Med cells were seeded in 96 96-well ULA plate (cat#7007, Corning Incorporated) at very low cell density in their culture media supplemented with 0.25% methylcellulose (cat#M7027, Sigma-Aldrich), as previously described.[57] After 72 h, spheroids were co-cultured with NK cells at different E:T ratios for additional 24 or 48 h. Spheroid growth and NK cell-mediated cytotoxicity were checked at various time points using the Celigo Image Cytometer (Nexcelom Bioscience), a microplate-based multichannel automated imaging system, to evaluate changes in area and fluorescence intensity.[58] NK cell cytotoxic potential against treated spheroids was assessed using a Cytoflex LX flow cytometer (Beckman Coulter) following PI staining.

3D cytotoxic assay

PDOs were grown in a Matrigel matrix for 5 days, and then the NK cells were added to the medium. NK cells and PDO were co-cultured for 72 hours in the IncuCyte SX5 Live-Cell Analysis System. The assay plate scan was scheduled every 24 hours. The ability of NK cells to migrate to PDO and kill them was evaluated by measuring the PDO area at different time points using the ImageJ software.

In vivo experiments

To investigate the in vivo antitumor activity of ^{ex}PD1-NK cells, leukemia and neuroblastoma mice tumor models were used. NALM-18-FF/GFP cells were intravenously (i.v.) injected (0.25×10^6 cells), in 6–8-week-old female NSG mice (NOD.Cg-Prkdcscid Il2rgtm1Wjl/SzJ; from Charles River). In a solid tumor setting, immunodeficient NSG mice were subcutaneously or orthotopically engrafted with SK-N-AS FF/GFP neuroblastoma. For the orthotopic MB models, D283-Med FF/GFP ($15x10^4$) cells were injected in the cerebellum of NSG mice (intracranial) using stereotaxic, as previously described.[59] After tumor engraftment, the mice received an i.v. injection of ^{ex}PD1-NK cells or mock-NK cells ($7x10^6$/mouse) harvested, washed, and resuspended in PBS 1X. Untreated mice served only as negative controls and received an i.v. injection of an equal volume of PBS 1X. Tumor growth was evaluated using the IVIS imaging system (PerkinElmer, USA) or the caliper. The intensity of the signal was measured every week as total photons/sec/cm2/sr (p/s/cm2/sr), as previously described.[60] Mice were maintained in the animal facility at Plaisant Castel Romano (Rome, Italy). All in vivo experiments complied with the

ethical international, EU, and national requirements and were approved by an ethical committee (Italian Health Ministry N°88/2016-PR and 805/2024-PR). Mice were matched based on the tumor signal for control and treatment groups before infusion of mock or ^{ex}PD1-NK cells. To compare the growth of tumors over time, bioluminescence signal intensity or tumor size measured with a caliper was collected blindly. Bioluminescence signal intensity was log-transformed and then compared using a two-sample t-test. In addition to tumor growth kinetics, in order to evaluate the toxicity of treatments, animal welfare was carefully assessed on a daily basis by trained personnel using standardized clinical scoring criteria, including body weight loss, posture, mobility, coat condition, food and water intake, and signs of pain or distress. Peripheral blood was collected from tumor-bearing mice treated or not with mock- or ^{ex}PD1-NK cells at different time points. Blood samples were processed to obtain serum, and biochemical analyses were performed to assess: aspartate aminotransferase (AST), alanine aminotransferase (ALT), alkaline phosphatase (ALP), albuminemia, total bilirubin, creatinine, and lactate dehydrogenase (LDH) by Plaisant Castel Romano (Rome, Italy). At the end of the experiment, spleens were harvested, fixed, and processed for histological evaluation. Tissue sections were prepared from fixed tissue and subjected to hematoxylin and eosin (H&E) staining. Histological analysis was performed independently by two operators. The circulating human ^{ex}PD1-NK cells were evaluated at the end of the experiments in selected organs.

Proteomic analysis

Protein quantification was performed using mass spectrometry with a data-independent acquisition (DIA) approach. Proteins detected in at least 50% of samples in at least one experimental group were retained for downstream analysis. Normality of protein expression was assessed with the Shapiro-Wilk test. Proteins with a normal distribution (p-value > 0.05) were compared between groups using a parametric test such as limma,[61] which is a moderated Analysis of Variance (ANOVA) test, followed by Benjamini-Hochberg correction for multiple testing. Conversely, non-normally distributed proteins were analyzed with a non-parametric Wilcoxon-Mann-Whitney test. Pathway enrichment was performed on proteins with unadjusted p-values < 0.05 using the Gene Ontology category "biological processes" to provide a comprehensive overview of group-specific biological differences. Enrichment results were corrected for multiple testing using the Benjamini-Hochberg procedure. For each pathway, the Gene Ratio (number of proteins mapped to the pathway / total input proteins), Background Ratio (number of proteins in the pathway / total database proteins), and Count of mapped proteins were reported. Finally, Gene Set Enrichment Analysis (GSEA)[62,63] was calculated by the GSEApy Python package[64] to assess whether specific pathways were consistently up- or down-regulated between sample groups, providing insight into coordinated changes in protein expression.

Data acquisition from TCGA and TARGET

Gene expression and clinical data for 33 adult cancer types were retrieved from The Cancer Genome Atlas (TCGA) using the R/Bioconductor package TCGAbiolinks (v2.26.3). Expression data were downloaded from the Transcriptome Profiling category, specifically selecting the Gene Expression Quantification data type with the STAR-Counts workflow. The following TCGA projects were included: TCGA-LGG, TCGA-THYM, TCGA-KIRC, TCGA-PAAD, TCGA-SKCM, TCGA-TGCT, TCGA-BRCA, TCGA-SARC, TCGA-PCPG, TCGA-UVM, TCGA-ACC, TCGA-HNSC, TCGA-COAD, TCGA-LAML, TCGA-UCS, TCGA-GBM, TCGA-LIHC, TCGA-OV, TCGA-KIRP, TCGA-KICH, TCGA-READ, TCGA-THCA, TCGA-LUAD, TCGA-MESO, TCGA-CHOL, TCGA-PRAD, TCGA-STAD, TCGA-LUSC, TCGA-DLBC, TCGA-CESC, TCGA-ESCA, TCGA-BLCA, and TCGA-UCEC. Clinical data were retrieved independently using analogous procedures, querying the Clinical data category with the Clinical Supplement data type. In addition, pediatric tumor data were obtained from the TARGET (Therapeutically Applicable Research to Generate Effective Treatments) database using TCGAbiolinks. The following pediatric cancer projects were included: TARGET-NBL (Neuroblastoma), TARGET-RT (Rhabdoid Tumor), TARGET-WT (Wilms Tumor), TARGET-CCSK (Clear Cell Sarcoma of the Kidney), TARGET-ALL-P3, TARGET-ALL-P2, TARGET-ALL-P1 (Acute Lymphoblastic Leukemia phases 3, 2, and 1, respectively), TARGET-AML (Acute Myeloid Leukemia), and TARGET-OS (Osteosarcoma). Gene expression values in Transcripts Per Million (TPM) were extracted from transcript quantification files available for each TCGA/TARGET sample.

Gene signatures and scoring

We defined multiple custom gene signatures to capture distinct immunological and tumor-related programs from TCGA/TARGET RNA-seq data. Signature scores were calculated as the mean expression (TPM values) of all genes in each signature detected in a sample; if fewer than three genes were present, the score was set to NA to ensure robustness, otherwise the arithmetic mean was computed, providing a summary metric reflecting the overall activity of the biological program represented by each signature. An immune infiltration signature of 7 genes (CD8A, CD8B, CXCL9, CXCL10, IFNG, GZMB, PRF1) was used to estimate general immune cell infiltration and stratify tumor samples into "cold" and "hot" based on the first and the last quantiles. Tumor samples with scores at or below the 20th percentile were classified as "cold" (low immune infiltration). Conversely, those tumor samples at or above the 80th percentile were classified as "hot" (high immune infiltration). A more specific NK cell infiltration signature of 20 genes (KLRK1, NCAM1, KLRD1, KLRC1, KLRC2, KLRB1, GZMB, GZMA, GNLY, PRF1, FCGR3A, NKG7, XCL1, XCL2, TYROBP, IL2RB, ZAP70, SH2D1B, CD160, CD244) was used to reflect natural killer cell presence in the tumor. Finally, an immunosuppression signature of 18 genes (PDCD1, TIGIT, HAVCR2, CD96, KLRC1, LAG3, CISH, SOCS1, SOCS3, IL10RA, TGFBR2, EOMES, FOXP3, CEACAM1, BTLA, ZFP36, PRDM1, IKZF2) was employed to represent checkpoint and inhibitory immune regulation within the TME. The correlations between these signatures and PD-L1/HLA-E expression were assessed by Pearson correlation analysis.

Survival analysis

To assess the prognostic relevance of the selected ligand genes across cancers, we performed a Kaplan-Meier analysis. Clinical metadata, including vital status and time to death or last follow-up, were extracted from TCGA XML files and matched to gene expression quantifications (TPM values) obtained from RNA-seq data. For each tumor type, patients were stratified into "High" and "Low" expression groups based on the top and bottom quintiles (80th and 20th quantiles) of tumor ligand expression. Kaplan-Meier survival curves were generated for each tumor-ligand pair, and statistical significance was evaluated using the log-rank test. Only tumor-ligand combinations with sufficient sample size ($n \geq 10$ per group) were considered. In parallel, we fitted univariate Cox proportional hazards models to quantify the hazard ratio (HR) associated with high versus low expression of each ligand across tumors. The log10-transformed HRs were visualized in a heatmap to summarize survival trends, with significance (p-value < 0.05) annotated directly on the plot. This approach enabled cross-tumor comparison of ligand prognostic impact, highlighting context-specific survival associations.

DATA AVAILABILITY

All codes to download the data and used to support the findings of this study, within the main text and supplementary information, are available on GitHub: https://github.com/sforcell/gmNK.

ACKNOWLEDGEMENTS

The authors acknowledge Daniela Pende from IRCCS Azienda Ospedaliera Metropolitana, Genoa, Italy for providing some reagents, Maximilian Reichart from Department of Internal Medicine II, Klinikum rechts der Isar, Technische Universität München, Munich, Germany for providing PDO lines, and Marco Pezzullo from the histology facility at Bambino Gesù Children's Hospital IRCCS in Rome, Italy, for conducting immunohistochemistry experiments. The authors declare that financial support was received for the research activities and to cover the publication fee. This work was supported by "AIRC-Associazione Italiana per la Ricerca sul Cancro" (project no IG 2022 ID 27065 to PV and 5x1000 2018 ID 21147 to LM) and the Italian Ministry of Health with "Current Research funds" and RC-2025 OPBG to PFF. The study was also partially supported by "Elterninitiative Leukämie- und tumorkranker Kinder Würzburg e.V." (IC), "Aktion Regenbogen für Leukämie- und tumorkranke Kinder Main-Tauber e.V." (IC), Deutsche Forschungsgemeinschaft (Ref. 470198222) (IC), A Collaborative Pediatric Cancer Research Awards Program (Ref. ^{23}YIN41, 24IN25) (IC) and "Amici del Sorriso Association" (IC). This work was also partially supported by "CureSearch Young Investigator Awards in Pediatric Oncology Drug Development" to FN and "Fondazione Roche per la Ricerca Indipendente" to FN. FN's lab is also supported by "Associazione Italiana per la Ricerca sul Cancro" (My First Airc Grant -Ref. 27019), the Italian Ministry of University and Research (PRIN-PNRR P2022JLHZZ), the Italian Ministry of Health (GR-2019-12369231), and the MIA NERI Foundation. SF was supported by a fellowship from the "Umberto Veronesi" Foundation (FUV). MTB was supported by an AIRC fellowship.

AUTHOR CONTRIBUTIONS

P.F.F. and P.V. conceived the ideas and designed the study. P.F.F., S.V., M.T.B., L.W.S., and M.R.A. performed the in vitro experiments. N.T., M.G., F.N., and P.V. designed and analyzed in vivo experiments. P.O. performed NKG2A-scFv isolation. I.C., M.M., T.S., and D.H. designed and validated the γ-retroviral vectors in vitro, as well as provided the γ retroviral supernatants for both in vitro and in vivo experiments. S.F. performed the bioinformatics analyses. L.M. and N.T. provided critical input on the project. P.F.F., S.F., L.M., N.T., I.C., and P.V. authors contributed to writing and reviewing the manuscript. All authors have read and approved the final manuscript.

ADDITIONAL INFORMATION

Supplementary information The online version contains supplementary material available at https://doi.org/10.1038/s41392-026-02827-w.

Competing interests: The authors declare no competing interests.

Publisher's note Springer Nature remains neutral with regard to jurisdictional claims in published maps and institutional affiliations.

REFERENCES

1. Liu, S. & Zhang, Y. Challenges and interventions of chimeric antigen receptor-T cell therapy in solid tumors. *Chin. J. Cancer Res.* **35**, 239–244 (2023).
2. Johnson, A., Townsend, M. & O'Neill, K. Tumor microenvironment immunosuppression: a roadblock to CAR T-cell advancement in solid tumors. *Cells* **11** (2022).
3. Kankeu Fonkoua, L. A., Sirpilla, O., Sakemura, R., Siegler, E. L. & Kenderian, S. S. C. A. R. T cell therapy and the tumor microenvironment: Current challenges and opportunities. *Mol. Ther. Oncol.* **25**, 69–77 (2022).
4. Maalej, K. M. et al. CAR-cell therapy in the era of solid tumor treatment: current challenges and emerging therapeutic advances. *Mol. Cancer* **22**, 20 (2023).
5. Zhang, M. et al. Advances in cancer immunotherapy: historical perspectives, current developments, and future directions. *Mol. Cancer* **24**, 136 (2025).
6. Zugasti, I. et al. CAR-T cell therapy for cancer: current challenges and future directions. *Signal Transduct. Target Ther.* **10**, 210 (2025).
7. Qi, Y. et al. Natural killer cell-related anti-tumour adoptive cell immunotherapy. *J. Cell Mol. Med.* **28**, e18362 (2024).
8. Du, B. et al. CAR-T therapy in solid tumors. *Cancer Cell* **43**, 665–679 (2025).
9. Cappell, K. M. & Kochenderfer, J. N. Long-term outcomes following CAR T cell therapy: what we know so far. *Nat. Rev. Clin. Oncol.* **20**, 359–371 (2023).
10. Neelapu, S. S. et al. Chimeric antigen receptor T-cell therapy - assessment and management of toxicities. *Nat. Rev. Clin. Oncol.* **15**, 47–62 (2018).
11. Tumino, N. et al. Polymorphonuclear myeloid-derived suppressor cells impair the anti-tumor efficacy of GD2.CAR T-cells in patients with neuroblastoma. *J. Hematol. Oncol.* **14**, 191 (2021).
12. Lu, Y. & Zhao, F. Strategies to overcome tumour relapse caused by antigen escape after CAR T therapy. *Mol. Cancer* **24**, 126 (2025).
13. Wang, D. R., Wu, X. L. & Sun, Y. L. Therapeutic targets and biomarkers of tumor immunotherapy: response versus non-response. *Signal Transduct. Target Ther.* **7**, 331 (2022).
14. Wu, X. et al. Targeting MHC-I molecules for cancer: function, mechanism, and therapeutic prospects. *Mol. Cancer* **22**, 194 (2023).
15. Saetersmoen, M. et al. Targeting HLA-E-overexpressing cancers with a NKG2A/C switch receptor. *Med.* **6**, 100521 (2025).
16. Soltani, M., Abbaszadeh, M., Fouladseresht, H., Sullman, M. J. M. & Eskandari, N. PD-L1 importance in malignancies comprehensive insights into the role of PD-L1 in malignancies: from molecular mechanisms to therapeutic opportunities. *Clin. Exp. Med.* **25**, 106 (2025).
17. Mariotti, F. R. et al. PD-1 in human NK cells: evidence of cytoplasmic mRNA and protein expression. *Oncoimmunology* **8**, 1557030 (2019).
18. Pesce, S. et al. Identification of a subset of human natural killer cells expressing high levels of programmed death 1: A phenotypic and functional characterization. *J. Allergy Clin. Immunol.* **139**, 335–346 e333 (2017).
19. Liu, X. et al. Immune checkpoints HLA-E:CD94-NKG2A and HLA-C:KIR2DL1 complementarily shield circulating tumor cells from NK-mediated immune surveillance. *Cell Discov.* **10**, 16 (2024).
20. Peng, L., Sferruzza, G., Yang, L., Zhou, L. & Chen, S. CAR-T and CAR-NK as cellular cancer immunotherapy for solid tumors. *Cell Mol. Immunol.* **21**, 1089–1108 (2024).
21. Fisher, J. G., Doyle, A. D. P., Graham, L. V., Khakoo, S. I. & Blunt, M. D. Disruption of the NKG2A:HLA-E immune checkpoint axis to enhance NK cell activation against cancer. *Vaccines* **10**, 1–17 (2022).
22. Li, Y. et al. Unlocking the therapeutic potential of the NKG2A-HLA-E immune checkpoint pathway in T cells and NK cells for cancer immunotherapy. *J. Immunother. Cancer* **12**, 1–14 (2024).
23. Beelen, N. A., Valckx, V. T. C., Bos, G. M. J. & Wieten, L. Interfering with KIR and NKG2A immune checkpoint axes to unleash NK cell immunotherapy. *Best. Pr. Res Clin. Haematol.* **37**, 101568 (2024).
24. Karvouni, M. et al. Challenges in alphaCD38-chimeric antigen receptor (CAR)-expressing natural killer (NK) cell-based immunotherapy in multiple myeloma: Harnessing the CD38dim phenotype of cytokine-stimulated NK cells as a strategy to prevent fratricide. *Cytotherapy* **25**, 763–772 (2023).
25. Pietra, G. et al. Human natural killer cells: news in the therapy of solid tumors and high-risk leukemias. *Cancer Immunol. Immunother.* **65**, 465–476 (2016).
26. Nieto, Y. et al. Allogeneic NK cells with a bispecific innate cell engager in refractory relapsed lymphoma: a phase 1 trial. *Nat. Med* **31**, 1987–1993 (2025).
27. Marin, D. et al. Safety, efficacy and determinants of response of allogeneic CD19-specific CAR-NK cells in CD19(+) B cell tumors: a phase 1/2 trial. *Nat. Med.* **30**, 772–784 (2024).
28. Liu, E. et al. Use of CAR-Transduced Natural Killer Cells in CD19-Positive Lymphoid Tumors. *N. Engl. J. Med.* **382**, 545–553 (2020).
29. Ingegnere, T. et al. Human CAR NK cells: a new non-viral method allowing high efficient transfection and strong tumor cell killing. *Front. Immunol.* **10**, 957 (2019).
30. De Mitri, F. et al. Inhibition of autophagy enhances the antitumor efficacy of T/CAR T cell against neuroblastoma. *J. Exp. Clin. Cancer Res.* **44**, 185 (2025).
31. Wu, B., Zhang, B., Li, B., Wu, H. & Jiang, M. Cold and hot tumors: from molecular mechanisms to targeted therapy. *Signal Transduct. Target Ther.* **9**, 274 (2024).
32. Galassi, C., Chan, T. A., Vitale, I. & Galluzzi, L. The hallmarks of cancer immune evasion. *Cancer Cell* **42**, 1825–1863 (2024).
33. Lei, W. et al. Safety and feasibility of 4-1BB co-stimulated CD19-specific CAR-NK cell therapy in refractory/relapsed large B cell lymphoma: a phase 1 trial. *Nat. Cancer* **6**, 786–800 (2025).
34. Guo, Y. et al. IL-15 Superagonist-Mediated Immunotoxicity: Role of NK Cells and IFN-gamma. *J. Immunol.* **195**, 2353–2364 (2015).
35. Christodoulou, I. et al. Engineering CAR-NK cells to secrete IL-15 sustains their anti-AML functionality but is associated with systemic toxicities. *J. Immunother. Cancer* **9** (2021).
36. Lorenzini, T. et al. Rational design of PD-1-CD28 immunostimulatory fusion proteins for CAR T cell therapy. *Br. J. Cancer* **129**, 696–705 (2023).
37. Lu, C. et al. A novel chimeric PD1-NKG2D-41BB receptor enhances antitumor activity of NK92 cells against human lung cancer H1299 cells by triggering pyroptosis. *Mol. Immunol.* **122**, 200–206 (2020).
38. Wang, J. et al. Multispecific targeting of glioblastoma with tumor microenvironment-responsive multifunctional engineered NK cells. *Proc. Natl. Acad. Sci. USA* **118**, 1–12 (2021).
39. Kembuan, G. J., Kim, J. Y., Maus, M. V. & Jan, M. Targeting solid tumor antigens with chimeric receptors: cancer biology meets synthetic immunology. *Trends Cancer* **10**, 312–331 (2024).
40. Xie, N. et al. Neoantigens: promising targets for cancer therapy. *Signal Transduct. Target Ther.* **8**, 9 (2023).
41. Vivier, E. et al. Natural killer cell therapies. *Nature* **626**, 727–736 (2024).
42. Zhao, H. et al. Inflammation and tumor progression: signaling pathways and targeted intervention. *Signal Transduct. Target Ther.* **6**, 263 (2021).
43. Thorsson, V. et al. The immune landscape of cancer. *Immunity* **48**, 812–830 e814 (2018).

44. Romee, R. et al. Cytokine-induced memory-like natural killer cells exhibit enhanced responses against myeloid leukemia. *Sci. Transl. Med.* **8**, 357ra123 (2016).
45. Guillerey, C., Huntington, N. D. & Smyth, M. J. Targeting natural killer cells in cancer immunotherapy. *Nat. Immunol.* **17**, 1025–1036 (2016).
46. Andre, P. et al. Anti-NKG2A mAb is a checkpoint inhibitor that promotes anti-tumor immunity by unleashing both T and NK Cells. *Cell* **175**, 1731–1743 e1713 (2018).
47. van Hall, T. et al. Monalizumab: inhibiting the novel immune checkpoint NKG2A. *J. Immunother. Cancer* **7**, 263 (2019).
48. Riggan, L., Shah, S. & O'Sullivan, T. E. Arrested development: suppression of NK cell function in the tumor microenvironment. *Clin. Transl. Immunol.* **10**, e1238 (2021).
49. Tumino, N. et al. The tumor microenvironment drives NK cell metabolic dysfunction leading to impaired antitumor activity. *Int J. Cancer* **152**, 1698–1706 (2023).
50. Nava Lauson, C. B. et al. Linoleic acid potentiates CD8(+) T cell metabolic fitness and antitumor immunity. *Cell Metab.* **35**, 633–650 e639 (2023).
51. Felices, M. et al. Continuous treatment with IL-15 exhausts human NK cells via a metabolic defect. *JCI Insight* **3**, 1–14 (2018).
52. Knopf, P. et al. Acidosis-mediated increase in IFN-gamma-induced PD-L1 expression on cancer cells as an immune escape mechanism in solid tumors. *Mol. Cancer* **22**, 207 (2023).
53. Oyer, J. L., Gitto, S. B., Altomare, D. A. & Copik, A. J. PD-L1 blockade enhances anti-tumor efficacy of NK cells. *Oncoimmunology* **7**, e1509819 (2018).
54. Pallavicini, I. et al. LSD1 inhibition improves efficacy of adoptive T cell therapy by enhancing CD8(+) T cell responsiveness. *Nat. Commun.* **15**, 7366 (2024).
55. Caruana, I. et al. K562-Derived Whole-Cell Vaccine Enhances Antitumor Responses of CAR-Redirected Virus-Specific Cytotoxic T Lymphocytes In Vivo. *Clin. Cancer Res.* **21**, 2952–2962 (2015).
56. Fiore, P. F. et al. Different effects of NK cells and NK-derived soluble factors on cell lines derived from primary or metastatic pancreatic cancers. *Cancer Immunol. Immunother.* **72**, 1417–1428 (2023).
57. Roper, S. J. & Coyle, B. Establishing an in vitro 3D spheroid model to study medulloblastoma drug response and tumor dissemination. *Curr. Protoc.* **2**, e357 (2022).
58. Zhang, H. et al. Novel high-throughput cell-based hybridoma screening methodology using the Celigo Image Cytometer. *J. Immunol. Methods* **447**, 23–30 (2017).
59. Nazio, F. et al. Targeting cancer stem cells in medulloblastoma by inhibiting AMBRA1 dual function in autophagy and STAT3 signalling. *Acta Neuropathol.* **142**, 537–564 (2021).
60. Di Stasi, A., De Angelis, B. & Savoldo, B. Gene therapy to improve migration of T cells to the tumor site. *Methods Mol. Biol.* **651**, 103–118 (2010).
61. Ritchie, M. E. et al. limma powers differential expression analyses for RNA-sequencing and microarray studies. *Nucleic Acids Res.* **43**, e47 (2015).
62. Subramanian, A. et al. Gene set enrichment analysis: a knowledge-based approach for interpreting genome-wide expression profiles. *Proc. Natl. Acad. Sci. USA* **102**, 15545–15550 (2005).
63. Mootha, V. K. et al. PGC-1alpha-responsive genes involved in oxidative phosphorylation are coordinately downregulated in human diabetes. *Nat. Genet.* **34**, 267–273 (2003).
64. Fang, Z., Liu, X. & Peltz, G. GSEApy: a comprehensive package for performing gene set enrichment analysis in Python. *Bioinformatics* **39**, 1–3 (2023).